

## Response to comments of Rev. 1

### MINOR POINTS:

5 L104: compare -> compares

Change done.

L200: although not necessary, I suggest a Table to summarize the experiment setups.

10 Yes, we thought of it and finally decided against it because there are already 3 tables in the paper. But we reformulated the description of the experiments to make it clearer.

L249: the choice of the radius of maximum wind as the radius to be used for the Hart diagram is not convincing. In my opinion, this represents a strong underestimation of the cyclone extension. I suggest to remove this point, or give a better motivation.

15 Considerations about the cyclone size, its time evolution and the period when it is representative of the symmetry of the event have been added.

L269: weakens -> decreases

Change done

20

L278: ... no change of the maximum wind compared to the previous period

This is not what we meant, and we realized that the sentence was misleading. It has been reformulated: “maximum wind speed 8 m s<sup>-1</sup> lower”. Thank you for this.

25 L283, 396: ... in Figure ...

Done.

L325: □□ is missing

Done, thank you

30

L335: what do you mean with “neutral” wind?

The neutral wind (or equivalent neutral wind) is commonly used when computing surface turbulent fluxes and corresponds to the wind speed obtained in neutral conditions in the surface layer (i.e. using a

logarithmic wind profile rather than stratification functions). We replaced “neutral wind” by “equivalent  
35 neutral wind” and added a reference.

Caption Fig. 10: please indicate that the figure refers to the NOCPL run  
Done.

40 L373, 478: resulting from ...  
Done.

L374: precipitation areas ...  
Change done.

45 L377: add “(see Fig. 5a)” and the end of the paragraph  
Change done.

L385: northeastwards ...  
50 Change done.

L408: H is controlled ...  
Change done

55 Caption Figure 11a: which level is shown?  
First level of the model, this is now specified

Caption Figure 13: (d) refers to H, thus all panels should be changed  
Done, thank you for checking this.

60 L435: “levels closest to the 1500 m” appear contrasting with what is reported in Figure 17 caption (the  
size of the symbols is inversely proportional to altitude between 0 and 1000m)  
Yes, we realized that the caption was probably misleading. The final point of the particles is actually  
1500 m, the symbol size in the figure is constant between 1000 and 1500 m asl, and increases when the  
65 height decreases. This is now specified in the caption.

L443: does the decrease in mixing ratio imply condensation and latent heating? In which way?

What we meant here is that the net increase of  $\theta$  implies condensation. The decrease of the mixing ratio can be due to condensation or to other processes (precipitation).

70

L491: “and there is no real PV tower around the cyclone centre”: be careful because this is not a general result, and it does not refer necessarily to cyclone of the first category. I think this sentence can make some confusion and I strongly suggest to remove it.

Done, thank you.

75

L492: “extending up to 800 hPa”: really, the warm core extends also in the upper troposphere; do you mean 400 hPa?

Yes, we changed this.

80 L502: ... is not due exclusively to ... but also to ...

Change done.

85

### Major comments

1) Drastic English Improvement. I think it is very important to improve significantly the English of this manuscript (sentences directly translated from the language of the authors to English, sentences too long and confusing, swap sentences, etc.). The fact the manuscript is not well-written distracts the reader from the content of the paper and also makes sometimes very difficult to understand what the authors are trying to communicate. The reader should not try to figure out what the authors are trying to explain. I understand that the Authors could not be native English speaker (as myself), so maybe a little help would be beneficial.

The text has been checked and rewritten almost entirely. We tried to improve the English, shorten the sentences and make it clearer overall. We hope that the present version is clear enough and does not prevent understanding the details of the scientific content.

2) The second critical aspect I am concern about is the fact that the control simulation the authors are using does not verify accurately the observations (e.g., Fig.3 and Fig. 4), from the tracking and intensity point of view of the medicane. Is this simulation the best simulation they can produce with this couple model? How many simulations the authors have performed in order to obtain the ‘best’ simulation that resemble the observations? Sometimes, this process can carry out more than 30 simulations changing different parameters of the model setup... Following this, if our control simulation cannot describe properly the observations, what is the point of using this simulation to describe the physical processes involved, in this case, in the medicane? In this case, the results and conclusions obtained do not properly describe the phenome we observe, they describe something else...

We made 8 tests in order to improve our track, and using the results of Cioni et al (2018) for instance. Several tests concern the time of initialization of the run on the larger domain, and the best result (used in this work) was obtained starting the run at 18:00 UTC on 6 November. The large scale is known to largely control the track of tropical cyclone, so most of our tests were about the influence of the initial conditions. We also tested a configuration very close to the one of Cioni et al. (2018), with no grid nesting (using directly the ECMWF forcing on the smaller domain), and a horizontal resolution of 2 km. This simulation gave a much better track, but the intensification and tropical transition of the cyclone was missed. We think that this difference is due to a different physics in the models used. We also increased the number of vertical levels, as this is known to impact the track of tropical cyclones, but the difference was not significant. Besides, Di Muzio et al. (2019) showed that the predictability of this medicane 48 h to 24 h before its maximum intensity is low compared to other events (especially its track, and its central pressure). This confirms the results of our tests, i.e. obtaining both accurate track and intensity is challenging. We chose the configuration with the best intensity, and checked that the time evolution and impacts of the event is close to observation. Note also that an error of 48 to 54 nautical miles (89 to 100 km) represents a rather good score for the NHC tropical cyclone forecast at 36 h lead time (see <https://www.nhc.noaa.gov/verification/verify4.shtml?>). We are then confident in the capacity of our simulation to represent the physical processes and the effect of coupling during this event.

3) Also, I found this manuscript too long, taking into account that this case study has been studied and examined by other authors before and most of the information described in this paper confirm previous results, conclusions or explanations. I think that in some sections, the information provided is not relevant, so they could resume significantly some of these sections.

130 Some sections have been notably shortened, especially the sections presenting results (4 Role of surface fluxes and mechanisms) and the conclusion/discussion.

4) Finally, in the conclusion section, the authors include new discussion about different categories where medicanes could be sorted. I think that this information should be introduced in one of the first sections of the manuscript and not at the conclusions. Again, in this last section, authors should try to  
135 overview the content and not repeat excessively content explained before.

Part of the information presented in the discussion has been move to the introduction, following this recommendation.

### Minor comments

#### Introduction

140 1) Page 1 (L1): I suggest to add some more references on Medicanes. This section is focussed on the description of the characteristics of Medicanes, but I feel that relevant references related with the definition of MEDICANES (acronym from Mediterranean Hurricane) are missing. Also, in the text the word medicane is related with mediterranean cyclones, and although the idea is clear, is not the definition used in the literature.

145 Yes, this has been clarified, and references have been added.

2) Page 1 (L27): “their radius ranges typically” -> “their radius typically ranges”

#### Change done

3) Page 1 (L28): “due to the enclosed **character** of the Mediterranean”. What do you mean by character? I realized that the way of explaining the differences between Medicanes and TC (L25-34) is  
150 not very clear because of the use of long sentences separated by semicolons. I suggest to rephrase these ideas in a clearer way to facilitate the reader its comprehension.

What was meant is that as the Mediterranean is composed of several basins of small size, cyclone tracks rapidly encounter the coast and decay. We reformulated. We also rephrased the comparison between medicanes and TCs.

155 4) Page 1 (L35-37) state that several studies documented different characteristics from medicanes, but only 1 reference is listed for each of these characteristics. I suggest to add more references.

#### Done

5) Page 2 (L41): “impact ot the coastal reliefs in triggering deep convection...” -> Add references

#### Done

160 6) Page 2 (L44-45): “It is nevertheless inadequate to ...” -> This sentence it seems completely disconnected from the last sentence, which talks about the adapted version of the Hart Diagram. What do the authors mean stating that is inadequate to describe roles of upper-level and low-level processes? Do they mean that upper-level dynamics do not play a key role in the genesis of medicanes? I suggest to add some additional clarification of the meaning of this sentence.

165 This part has been removed from the Introduction.

7) Page 2 (L59-61): Add more references.

Done

170 8) Page 2 (L65): “turning off selected processes in sensitivity experiments”-> In fact, the factor separation technique is a method of performing sensitivity experiments turning on/off different factors considered.

Yes, thank you, this has been corrected.

9) Page 3 (L84): “latent heat release **fed** at low level” -> It is not clear for me that this term can be used in this context.

175 This has been reformulated

Case study and simulations

1) Page 4 (L125-126): “with high horizontal (1-2 km)” -> “with high **grid** horizontal and ... resolutions”

Change done

180 2) Page 4 (L126): “present” -> “current”?

Change done

3) Page 4 (L127): “platforms” -> “centers”?

Change done

4) Page 5 (L162): “radiative transfers” -> “radiative transfer models”

185 Change done

5) Page 5 (L172): “ECMWF operational analyses” -> Please, provide more information about these fields.

Done

6) Page 5 (L177): “with resolution 1.33 km” -> “with **grid** resolution 1.33 km”

190 Change done

7) Page 6 (L199): “configurations described previously” -> “configurations previously described”

Change done

Medicane lifecycle and coupling impact

1) Page 7 (L266): “until its landfall” -> “until it makes landfall”?

195 [Change done](#)

2) Page 7 (L271): “collocated” -> “located”?, “placed”?

[What we meant here is that the upper level PV anomaly and the SLP minimum are aligned. We reformulated.](#)

Role of surface fluxes

200 1) Page 9 (L325-328): Too long sentence.

[We reformulated](#)

Figures:

Most of the figures are poor quality. I suggest to create .pdf or .eps format figures to increase quality of the manuscript.

205 [All the figures were redone in pdf format.](#)

Fig. 7: missing x and y labels.

[Corrected](#)

Fig. 8-9-10. Misleading x-label. It should be replace with something such as: Time (hours UTC)

[Change done](#)

210 Fig. 11: Dashed line representing cross section region and the grey star should be highlighted. In addition, in the capture, the last line should be corrected to “Grey stars indicate the position...” instead of “**The** grey stars indicate the position...”

[Changes done](#)

Fig. 12,14: missing x-label

215 [Change done](#)

Fig. 13, 16, 18: Coast lines are too width and difficult the visualization of the fields depicted. Please, improve this feature. Also, enlarge grey stars.

[Changes done](#)

Fig. 17: Enlarge grey star.

220 [Change done](#)

# Surface processes in the 7 November 2014 medicane from air-sea coupled high-resolution numerical modelling

225 Marie-Noëlle Bouin<sup>1,2</sup>, Cindy Lebeaupin Brossier<sup>1</sup>

<sup>1</sup>CNRM, Université de Toulouse, Météo-France, CNRS, Toulouse, France

<sup>2</sup>Laboratoire d'Océanographie Physique et Spatiale, Ifremer, University of Brest, CNRS, IRD, Brest, France

*Correspondence to:* Marie-Noëlle Bouin (marie-noelle.bouin@meteo.fr)

**Abstract.** A medicane, or Mediterranean cyclone with characteristics similar to tropical cyclones, is simulated using a  
230 kilometre-scale ocean-atmosphere coupled modelling platform. A first phase leads to strong convective precipitation, with  
high potential vorticity anomalies aloft due to an upper-level trough. Then, the deepening and tropical transition of the  
cyclone result from a synergy of baroclinic and diabatic processes. Heavy precipitation ~~result~~<sup>result</sup> from uplift of  
conditionally unstable air masses due to low-level convergence at sea. This convergence is enhanced by cold pools,  
~~generated~~<sup>resulting</sup> either ~~by~~<sup>from</sup> rain evaporation or ~~by~~<sup>from</sup> advection of continental air masses from North Africa.  
235 Backtrajectories show that air-sea heat exchanges moisten the low-level inflow towards the cyclone centre. However, the  
impact of ocean-atmosphere coupling on the cyclone track, intensity and lifecycle is very weak. ~~This is;~~ due to a sea surface  
cooling one order of magnitude weaker than for tropical cyclones, even on the area of strong enthalpy fluxes. Surface  
currents have no impact. Analysing the surface enthalpy fluxes shows that evaporation is controlled mainly by the sea  
surface temperature and wind. Humidity and temperature at first level play a role during the development phase only. In  
240 contrast, the sensible heat transfer depends mainly on the temperature at first level throughout the medicane lifetime. This  
study shows that the tropical transition, in this case, is dependent on processes widespread in the Mediterranean Basin, like  
advection of continental air, rain evaporation and formation of cold pools, and dry air intrusion.

## 1 Introduction

Medicanes are small-size Mediterranean cyclones presenting, during their mature phase, characteristics similar to those of  
245 tropical cyclones. ~~including~~ <sup>This includes</sup> a cloudless and almost windless column at their centre ~~looking like a cyclone eye,~~  
spiral rain bands and a large-scale cold anomaly surrounding a smaller warm anomaly ~~at their centre,~~ extending at least up to  
the mid troposphere (~400 hPa, Picornell et al., 2014). However, they differ from their tropical counterparts by many  
aspects. ~~First,;~~ their intensity is much weaker, with maximum wind speed reaching those of tropical storms, or Category 1  
hurricane on the Saffir–Simpson scale for the most intense of them (Miglietta et al., 2013). ~~Second,;~~ <sup>they are much smaller</sup>  
250 ~~with;~~ <sup>typical</sup> radius ~~ranges typically from~~ 50 to 200 km (Picornell et al., 2014). ~~Third, their mature phase lasts a few~~  
~~hours to 1 to 2 days because due to the enclosed character of the Mediterranean Sea leading rapidly to the small size of the~~  
~~Mediterranean basin leads them to~~ landfall ~~rapidly,~~ and ~~because~~ <sup>to</sup> the ~~limited~~ ocean heat capacity ~~is weak,~~ <sup>the duration of</sup>  
~~their mature phase vary from a few hours to 1 to 2 days,;~~ <sup>Fourth,</sup> ~~they are able to~~ develop and sustain over sea surface  
temperature (SST) typically 15 to 23 °C (Tous and Romero, 2013), much colder than the 26 °C threshold of tropical  
255 cyclones (Trenberth, 2005; although tropical cyclones formed by a tropical transition can develop over colder water,  
McTaggart-Cowan et al. 2015). ~~and Finally, a development phase including at their early stage,~~ vertical wind shear and  
horizontal temperature gradient ~~are~~ <sup>is</sup> necessary ~~to the early stage of~~ their development ~~and the establishment of deep~~  
~~convection~~ (e.g. Flaounas et al., 2015).

In the last decade, several studies ~~investiga~~<sup>documented</sup> their characteristics and conditions of formation, either from satellite  
260 observations (~~Claud et al., 2010;~~ Tous and Romero, 2013), climatological studies (~~Gaertner et al., 2007;~~ Cavicchia and



Gualdi, 2014; Flaounas et al., 2015), or case studies based on simulations (Davolio et al., 2009; Miglietta et al., 2013; 2017; Miglietta and Rotunno, 2019). ~~A~~From these studies, a feature common to many medicanes is the presence of an elongated upper-level trough (also known as a “PV streamer”) bringing cold air with high values of potential vorticity (PV) from higher-latitude regions. Other local effects favouring their development are: lee cyclones forming south of the Alps or north of the North African reliefs (Tibaldi et al., 1990), ~~the impact of the~~ coastal reliefs ~~favouring in triggering~~ deep convection (Moscatello et al., 2008); and relatively warm sea surface waters able to feed the process of latent heat release during their mature phase. Among Mediterranean cyclones, the classification of Hart (2003) established for tropical cyclones and adapted to the Mediterranean conditions (Picornell et al., 2014), helps to reliably identify warm core, symmetric events. It is nevertheless inadequate to describe the respective roles of upper-level and low-level processes (e.g. surface heat exchanges or role of geographical conditions like orographic lifting).

The medicane cases ~~meeting all the previous criteria confirmed by converging characteristics as those mentioned above~~ represent only a small portion of the Mediterranean cyclones (e.g. 13 over 200 cases of intense cyclones ~~or roughly one per year~~ in the study of Flaounas et al., 2015, ~~or roughly one per year~~). Due to this scarcity, ~~clearly defining isolating in a definite way~~ the ~~properties characteristics~~ enabling to separate medicanes from other Mediterranean cyclones ~~is still challenging proved elusive~~. A study using dynamical criteria concluded that medicanes are very similar to other intense cyclones, with a slightly weaker upper-level and a stronger low-level PV anomalies (Flaounas et al., 2015). Recent comparative studies (e.g. Akhtar et al., 2014; Miglietta et al., 2017) showed a large diversity of duration, extension (size and vertical extent) and characteristics (dominating role of baroclinic versus diabatic processes) within the medicane category.

~~T~~Despite such a context, the role of the large-scale environment like the PV streamer and of the associated upper-level jet ~~in medicane formation~~ has been the subject of several studies (Reale and Atlas, 2001; Homar et al., 2006; Flaounas et al., 2015; Carrió et al., 2017). On a case study in September 2006, it was shown for the first time that the crossing of the upper-level jet by the cyclone ~~to the left exit of the jet~~ resulted in ~~its a~~ rapid deepening ~~of the surface low-pressure system~~ by interaction between low-troposphere and upper-level PV anomalies (Chaboureaud et al., 2012). Recently, the ubiquitous presence of PV streamers and their key role in the ~~baroclinic~~ development of the medicanes have been confirmed ~~by a study based on simulations and satellite analyses of on~~ several cases ~~of intense medicanes~~ (Miglietta et al., 2017). ~~These studies emphasized the importance of the large-scale conditions prior to the development of the cyclone.~~ These studies concluded also that, during their lifecycle, medicanes can rely either on purely diabatic processes or on a combination of baroclinic and diabatic processes (Mazza et al., 2017; Fita and Flaounas, 2018; Miglietta and Rotunno, 2019).

Conversely, the investigation of the contribution of surface processes has motivated ~~less few studies so far~~. Some of them aimed at ~~assessing~~ the relative importance of surface heat extraction versus latent heat release and upper-level PV anomaly throughout the cyclone lifetime, by using adjoint models, ~~or factor separation techniques, or turning off selected processes in sensitivity experiments~~ (Reed et al., 2001; Homar et al., 2003; Moscatello et al., 2008; Carrió et al., 2017). They concluded that, ~~whereas~~ the presence of the upper-level trough during the earlier stage of the cyclone and the latent heat release during its developing and mature phases are necessary. ~~In contrast, to its deepening and maintenance,~~ the role of surface heat fluxes is more elusive. Like in tropical cyclones, the latent heat fluxes always dominate the surface enthalpy processes ~~(, with the~~ sensible heat fluxes ~~representing~~ 25 to 30 % of the turbulent ~~heat~~ fluxes prior to the tropical transition, and 15 to 20 % during the mature phase. ~~(Pytharoulis, 2018)~~. Early studies ~~using simulations first~~ concluded that low-level instability controlled by surface heat fluxes may be “an important factor of intensification” (Reed et al., 2001, case of January 1982) and that the latent heat extraction from the sea is a “key factor of feeding of the latent-heat release” (Homar et al., 2003, case study of September 1996). Turning off the surface turbulent fluxes during different phases of the cyclone brought contrast to this view. ~~showing that~~ Indeed, the role of surface enthalpy in feeding the cyclonic circulation ~~is not constant throughout its~~

lifecycle. Indeed, it revealed important during its earliest and mature phases, ~~whereas its role playing only a~~ marginal role during the deepening (Moscattello et al., 2008, case study of September 2006).

More recently, studies simulating several cyclones suggested that the impact of the surface fluxes on the cyclone are probably case-dependent (Tous and Romero, 2013; Miglietta and Rotunno, 2019). The latter ~~work study~~ especially compared the medicanes of October 1996 (between the Balearic Islands and Sardinia) and December 2005 (north of Libya) ~~to investigate the relative using the same modelling platform. Sensitivity studies performed with and without surface fluxes showed contrasted results, which were attributed to the different competing roles of~~ played by the WISHE-like mechanisms (Wind Induced Surface Heat Exchange: Emanuel, 1986; Rotunno and Emanuel, 1987) ~~and versus~~ baroclinic processes ~~in the two cases. In both cases, high upper-level PV values play a strong role in the initiation of the cyclone. The major difference comes from the role of surface fluxes.~~ In the case of October 1996, the cyclone warm core is formed by latent heat release fed at low level by ~~sea-surface heat fluxes~~ heat and moisture extracted from the sea. ~~Surface fluxes are above 1500 W m<sup>-2</sup> over large areas due to persistent orographic winds bringing cold and dry air for several days prior to the cyclone development, that contribute to destabilize the surface layer. The features characteristics of tropical cyclones are well marked: warm core extending up to 400 hPa, symmetry, low-level convergence and upper-level divergence, and strong contrast of equivalent potential temperature  $\theta_e$  ( $\sim 8$  °C) between the surface and 900 hPa as an evidence of latent heating. In the December 2005 case, the warm core is due to warm air seclusion. the cyclone develops within a large-scale baroclinic environment, with the PV streamer slowly evolving into a cut-off low. The tropical-like features are less evident: weaker warm core due to warm air seclusion, weaker gradient of  $\theta_e$  ( $\sim 3$ – $4$  °C) between the surface and 900 hPa. The surface enthalpy fluxes play only a marginal role and peak around 1000 W m<sup>-2</sup> for a few hours.~~ The authors concluded that ~~different categories of intensification mechanisms leading to medicanes co-exist. This suggests that~~ mechanisms of transition towards tropical-like cyclones are diverse, especially concerning the role of the air–sea heat exchanges.

As surface fluxes may strongly depend on the SST, a change of the oceanic surface conditions may, in theory, impact the development of a medicane. Several sensitivity studies investigated the impact of a uniform SST change on the cyclone ~~development and lifecycle~~, for instance to anticipate the possible effect of the Mediterranean surface waters warming due to climate change. Consistent tendencies were obtained on different case studies (Homar et al., 2003, case of September 1996; Miglietta et al., 2011, case of September 2006; Pytharoulis, 2018, case of November 2014; Noyelle et al., 2019, case of October 1996), ~~showing that, As~~ expected, warmer (respectively colder) SSTs lead to more (resp. less) intense cyclones ~~even though. However,~~ changes of SST by less than  $\pm 2$  °C result in no significant change in the track, duration or intensity of the cyclone.

The impact of coupling atmospheric and oceanic models has been studied mainly using regional climate models on seasonal to interannual time scales. Comparing coupled and non-coupled simulations ~~using a regional climate model~~ showed an impact of the coupling ~~when provided~~ the horizontal resolution of the model is at least  $0.08^\circ$  (Akhtar et al., 2014). This resolution ~~is proved~~ also necessary to reproduce in a realistic way the characteristic processes of medicanes, including warm cores, and strong winds at low level. Coupled simulations resulted in more intense latent and sensible heat surface fluxes, contrasting with what is usually obtained in tropical cyclones due to the strong cooling effect of the cyclone on the sea surface (Schade and Emanuel, 1999; D'Asaro et al., 2007). This can be due to the use of a 1D ocean model and its limited ability to reproduce the oceanic processes responsible of the cooling. The ~~need of higher resolution consideration about the resolution needed~~ to observe an impact of the ~~couplings surface processes~~ was confirmed by ~~the results of~~ Gaertner et al. (2017), or Flaounas et al. (2018). Both studies compare ~~ds~~ several simulations at the seasonal or interannual scale, both coupled and uncoupled and from several regional climate modelling platforms. ~~No clear impact of the coupling on the cyclones intensity was evidenced. The but the authors attributed this~~ lack of impact ~~they obtained was attributed~~ to the

relatively low horizontal resolution of the ~~simulation coupled experiments~~, between 18 and 50 km. Finally, a case study ~~based on comparing~~ higher-resolution (5 km) ~~coupled and uncoupled~~ simulations of the medicane of November 2011 showed no strong impact of the surface coupling. ~~The SST with a weak decrease of the SST of was 0.1 to 0.3°C lower only, the SLP minimum was 2 hPa higher and a difference of 2 hPa on the minimum of SLP and the maximum surface wind 5 m s<sup>-1</sup> lower on the surface wind speed~~ (Ricchi et al., 2017). The impact of ocean–atmosphere coupling in high-resolution (~ 1–2 km), convection-resolving models has, to the best of our knowledge, not been ~~evaluat~~assessed yet.

In the present study, we assess the feedback of the ocean surface on the atmosphere ~~in the case~~ of the medicane of November 2014 (also known as Qendresa) ~~over the Strait of Sicily and Ionian Sea~~ using a kilometre-scale ocean–atmosphere coupled model. We investigate the role of the surface processes, especially during the mature phase of the medicane, and we examine the role of the different parameters (including SST) controlling these fluxes throughout the lifecycle of the cyclone.

A brief description of the medicane, ~~and the description~~ of the modelling tools and ~~of the~~ simulation strategy are given in Sect. 2. In Section 3, the results of the reference simulation are used to describe the medicane characteristics and lifecycle ~~with its different phases~~ and to present the impact of the coupling. The role of the surface conditions and mechanisms controlling the air–sea fluxes ~~are assessed~~ during the different phases ~~are assessed~~ in Sect. 4. These results are discussed in Sect. 5, and some conclusions are given.

## 2 Case study and simulations

The case study is the Qendresa medicane that affected the region of Sicily on 7 November 2014. It has been the subject of several studies based on simulations. ~~They, either~~ investigat~~ed~~ing the role of SST anomalies or the impact of ~~a~~ uniform SST change (Pytharoulis, 2018), the respective role of upper-air instability, surface exchanges and latent heat release (Carrió et al., 2017) or the predictability of the event, depending on the initial conditions and horizontal resolution of the model (Cioni et al., 2018). All those studies showed that the predictability of this event and especially of its track is rather low, even with high horizontal (1–2 km) and vertical (50 to 80 levels) ~~grid~~ resolutions of ~~curr~~present operational numerical weather prediction (NWP) ~~centre~~platforms. A recent study based on the ensemble forecasts of the ECMWF (European Centre for Medium-Range Weather Forecasts, Di Muzio et al., 2019) showed that the predictability of occurrence (with respect to the operational analysis) is good as early as 7.5 days lead time, but the predictability of the position is weak, especially between 4 and 1 days lead time (their Fig. 6). The predicted central pressure is also consistently 10 to 14 hPa higher than the analysed one, whatever the lead time considered.

### 2.1 The 7 November 2014 medicane

On 5 and 6 November 2014, a PV streamer extended from Northern Europe to North Africa, bringing cold air ( $-23$  °C) and enhancing instability aloft. A general cyclonic circulation developed over the Western Mediterranean basin while Eastern Mediterranean was dominated by high pressures (Fig. 1a). At low level on 6 November, the cold and warm fronts associated with the baroclinic disturbance reinforced due to a northward advection of warmer and moist air; from North Africa (Fig. 1b). The system moved towards the Sicily Strait and deepened during the night of 6 to 7 November. On the early hours of 7 November, the upper-level PV trough and the low-level cyclone progressively aligned (Fig. 1c), reinforcing the PV transfer from above and the low-level instability. Strong convection developed, with heavy precipitation in the Sicily area. The low-level system rapidly deepened in the morning of 7 November, with a sudden drop of 8 hPa in 6 hours, and evolved to the quasi-circular structure of a tropical cyclone with spiral rain bands and a cloudless eye-like centre. The maximum intensity was reached around 12:00 UTC on 7 November north of Lampedusa (see Fig. 3 for main place names). The system drifted eastwards ~~and~~ slowly weaken~~ed~~ing during the afternoon of the 7 November with a first landfall at Malta around 17:00. ~~It~~

then moved northeastwards to reach the Sicilian coasts in the evening. It ~~then~~ continued its decay during the following night close to the Sicily coasts, and lost its circular shape and tropical cyclone appearance around 12:00 UTC on 8 November.

## 2.2 Simulations

385 Three numerical simulations of the event were performed using the state-of-the-art atmospheric model Meso-NH (Lac et al., 2018) and the oceanic model NEMO (Madec and the NEMO Team, 2016).

### 2.2.1 Atmospheric model

The non-hydrostatic French research model Meso-NH version 5.3.0 is used here with a fourth-order centered advection scheme for the momentum components and the piecewise parabolic method advection scheme from Colella and Woodward  
390 (1984) for the other variables, associated with a leapfrog time scheme. A C grid in the Arakawa convention (Mesinger and Arakawa, 1976) is used for both horizontal and vertical discretizations, with a conformal projection system of horizontal coordinates. A fourth-order diffusion scheme is applied to the fluctuations of the wind variables, which are defined as the departures from the large-scale values. The turbulence scheme (Cuxart et al., 2000) is based on a 1.5-order closure coming from the system of second-order equations for the turbulent moments derived from Redelsperger and Sommeria (1986) in a  
395 one-dimensional simplified form assuming that the horizontal gradients and turbulent fluxes are much smaller than their vertical counterparts. The mixing length is parameterized according to Bougeault and Lacarrere (1989) who related it to the distance that a parcel with a given turbulent kinetic energy at level  $z$  can travel downwards or upwards before being stopped by buoyancy effects. Near the surface, these mixing lengths are modified according to Redelsperger et al. (2001) to match both the Monin–Obukhov similarity laws and the free-stream model constants. The radiative transfer is computed by solving  
400 long-wave and short-wave radiative transfer ~~models~~ separately using the ECMWF operational radiation code (Morcrette, 1991). The surface fluxes are computed within the SURFEX module (Surface Externalisée, Masson et al., 2013) using over sea the iterative bulk parametrization ECUME (Belamari et al., 2005; Belamari and Pirani, 2007) linking the surface turbulent fluxes to the meteorological gradients ~~and the SST~~ through the appropriate transfer coefficients. The Meso-NH model shares its physical representation of parameters, including the surface fluxes parametrization, with the French  
405 operational model AROME (Seity et al., 2011) used for the Météo-France NWP with a current horizontal grid spacing of 1.3 km. In this configuration, deep convection is explicitly represented while shallow convection is parametrized using the eddy diffusivity Kain–Fritsch scheme (Pergaud et al., 2009).

In the present study, a first atmosphere-only simulation with a grid spacing of 4 km has been performed on a larger domain of  $3200 \text{ km} \times 2300 \text{ km}$  (D1, see Fig. 2). This simulation started at 18:00 UTC the 6 November and lasted 42 h until 12:00  
410 UTC the 8 November. Its initial and boundary conditions come from the ECMWF operational analyses [Cy40R1 \(horizontal resolution close to 16 km, 137 vertical levels\)](#) every 6 h.

As described in the following, this 4 km simulation ~~then~~ provides initial and boundary conditions for simulations on a smaller domain of  $900 \text{ km} \times 1280 \text{ km}$  (D2, Fig. 2). This domain extension was chosen as a trade-off between computing time and an extension large enough to represent the physical processes involved in the cyclone lifecycle, including the  
415 influence of the coasts. All simulations on the inner domain D2 share [a time step of 3 s and](#) their ~~horizontal~~ grid (with [horizontal grid resolution of 1.33 km and](#)) ~~and vertical grid with 55 stretched terrain-following levels~~, ~~and a time step of 3 s~~. Atmospheric and surface parameter fields are issued every 30 minutes.

### 2.2.2 Oceanic model

The ocean model used is NEMO (version 3\_6) (Madec and the NEMO Team, 2016) with physical parametrizations as follows. The total variance dissipation scheme is used for tracer advection in order to conserve energy and enstrophy (Barnier et al., 2006). The vertical diffusion follows the standard turbulent kinetic energy formulation of NEMO (Blanke and Delecluse, 1993). In case of unstable conditions, a higher diffusivity coefficient of  $10 \text{ m}^2 \text{ s}^{-1}$  is applied (Lazar et al., 1999). The sea-surface height is a prognostic variable solved thanks to the filtered free-surface scheme of Roullet and Madec (2000). A no-slip lateral boundary condition is applied and the bottom friction is parameterized by a quadratic function with a coefficient depending on the 2D mean tidal energy (Lyard et al., 2006; Beuvier et al., 2012). The diffusion is applied along iso-neutral surfaces for the tracers using a Laplacian operator with the horizontal eddy diffusivity value  $\nu_h$  of  $30 \text{ m}^2 \text{ s}^{-1}$ . For the dynamics, a bi-Laplacian operator is used with the horizontal viscosity coefficient  $\eta_h$  of  $-1.10^9 \text{ m}^4 \text{ s}^{-1}$ .

The configuration used here is sub-regional and eddy-resolving, with a  $1/36^\circ$  horizontal resolution over an ORCA grid from 2.2 to 2.6 km resolution named SICIL36 (ORCA is a tripolar grid with variable resolution, Madec and Imbard, 1996), that was extracted from the MED36 configuration domain (Arsouze et al., 2013) and shares the same physical parametrizations with its “sister” configuration WMED36 (Lebeaupin Brossier et al., 2014; Rainaud et al., 2017). It uses 50 stretched  $z$ -levels in the vertical, with level thickness ranging from 1 m near the surface to 400 m at the sea bottom (i.e. around 4000 m depth) and a partial step representation of the bottom topography (Barnier et al., 2006). It has 4 open boundaries corresponding to those of the D2 domain shown in Figure 2, and its time step is set to 300 s. The initial and open boundary conditions come from the global  $1/12^\circ$  resolution PSY2V4R4 daily analyses from Mercator Océan International (Lellouche et al., 2013).

### 2.2.3 Configuration of simulations

The three-hourly outputs of the large-scale simulation on D1 were used as boundary and initial conditions for 3 different simulations on the smaller domain D2, based on the previously described atmospheric and oceanic configurations ~~described previously~~. These three simulations start at 00:00 UTC on 7 November and last 36 h until 12:00 UTC on 8 November. The first atmosphere-only simulation called NOCPL uses ~~a~~ fixed SST forcing, while the CPL and NOCUR simulations ~~are~~ the two-way coupled ~~simulation~~ between ~~the~~ Meso-NH and NEMO-SICIL36 ~~model~~. ~~Indeed, in CPL, the SURFEX-OASIS coupling interface (Voltaire et al., 2017) enables to exchange the SST and two-dimensional surface currents from NEMO to Meso-NH and the two components of the momentum flux, the solar and non-solar heat fluxes and the freshwater flux from Meso-NH to NEMO every 15 minutes. The NOCUR run is similar. To test the respective impact of the surface currents on the atmosphere with respect to the impact of the SST, another coupled simulation has been performed (NOCUR in the following). It is similar to CPL except that the surface currents are not transmit~~ exported from NEMO to Meso-NH.

In order to ensure that the impact of the coupling in the NOCUR and CPL configurations ~~originate~~ corresponds ~~from~~ to the time evolution of the SST rather than ~~from~~ to a change in the initial SST field, the SST field (~~shown in Fig. 3~~) used as a surface forcing in NOCPL ~~(and kept constant throughout the simulation)~~ is ~~the field~~ produced by the CPL run, 1 h after the beginning of the simulation (i.e. after the initial adjustment of the oceanic model). This field (Fig. 3) is kept constant throughout the simulation.

### 2.3 Validation

Figure 3 compares the tracks of Qendresa obtained in the three different simulations ~~with~~ ~~are compared to~~ the best track based on observations (brightness temperature from radiance in the  $10.8 \mu\text{m}$  channel measured by the SEVIRI instrument aboard the MSG satellite, see Cioni et al., 2018) ~~in Figure 3~~. All the simulated tracks are shifted northwards with respect to



the observations since the beginning of the simulations. The mean distance between the simulated and observed tracks is close to 85 km with no significant difference between the simulations. Cioni et al. (2018) showed that using horizontal resolutions finer than 2.5 km is mandatory to accurately represent the fine-scale structure of this cyclone and its time evolution. Sensitivity studies showed ~~that better resolution an increased convergence of results in~~ simulated track ~~closer~~  
460 ~~towards the~~ observations, ~~with higher resolution~~. The best agreement ~~is being~~ obtained with a nested configuration and an inner domain at 300 m resolution. In the present study, several sensitivity tests ~~based on these results~~ were performed on the smaller-domain ~~simulation~~ to improve the simulated track: i) the starting time of the simulation was changed between 12:00 UTC on 6 November and 00:00 UTC on 7 November with increment of 3 h; ii) the number of vertical levels in Meso-NH was increased to 100, with a stretching ensuring a better sampling in the atmospheric boundary layer; iii) the atmospheric  
465 simulation was performed without nesting, initial and boundary conditions from ECMWF, and horizontal resolution of 2 km. Note that our inner domain D2 is close in its extension to the domain used by Cioni et al. (2018). None of these tests ~~(8 in total) resulted in a~~ significantly improved ~~the~~ track, the northward shifting of the cyclone occurring in every case in the early hours of the 7 November.

The ~~simulated cyclone nevertheless shows a~~ deepening and maximum intensity ~~of the simulated cyclone are nevertheless~~  
470 close to the observed ones, even if a direct (i.e. co-localized) comparison is not possible due to the northward shift of its track. A strong deepening of almost 15 hPa is obtained in the first 12 h of the CPL simulation (Fig. 4b) with a minimum value at 12:30 UTC on the 7 November close to the minimum observed at Linosa station. This station ~~has been chosen as~~ the closest point to the best track ~~from observations~~ at the time of the observed maximum intensity of the storm. The surface wind speeds ~~show peaks values~~ at the same time (Fig. 4a), and ~~its~~ time evolution ~~in good~~ agrees ~~wellment~~ with METAR  
475 observations at the stations of Lampedusa, Pantelleria or Malta. ~~Also, the time evolution of the w~~ Wind speed averaged over a 50 km radius around the cyclone centre ~~presents a time evolution close to is in good agreement with~~ the control simulation of Cioni et al. (2018). ~~Despite the northward shift of its track, the medicane simulated by Meso-NH is very realistic and can be used to explore the processes at play, especially concerning the role of the sea surface thanks to the CPL simulation.~~

### 3 Medicane lifecycle and coupling impact

480 This part presents first the successive phases of the event based on an analysis of upper-level and mid-troposphere processes. Then, ~~we assess~~ the impact of ~~taking into~~ accounting ~~for~~ the short-time evolution of the SST on the atmospheric surface processes, ~~through ocean-atmosphere coupling, is assessed.~~

#### 3.1 Chronology of the simulated event

~~We used t~~ The successive phases of the medicane are examined using the methodology of Fita and Flaounas (2018) based on  
485 ~~its~~ upper-level and low-level dynamics, ~~and on its~~ asymmetry and thermal wind, ~~to characterize the phases of the medicane.~~ Figure 5 shows the 300 hPa PV anomaly, SLP, surface wind and equivalent potential temperature  $\theta_e$  at 850 hPa from the NOCPL simulation. ~~Moreover,~~ phase space diagrams are commonly used to describe in a synthetic way the symmetric characteristics of the cyclone, as well as the thermal characteristics and extent of its core. The present version in Figure 6 showing the evolution of Qendresa from 01:00 UTC on 7 November to 12:00 UTC on 8 November is derived from the  
490 original work of Hart (2003) using the adaptation of Picornell et al. (2014) for smaller-scale cyclones. The radius used for computing the low-troposphere thickness asymmetry  $B$ , the low-troposphere and upper-troposphere thermal winds ( $\rightarrow V_{TL}$  and  $\rightarrow V_{TU}$  respectively) has been fitted to the radius of maximum wind at 850 hPa and is close to 100 km, and the low troposphere and upper troposphere are defined here as the 925–700 hPa and 700–400 hPa levels respectively. ~~The radius~~

value of 100 km is in agreement with several other studies focusing on medicanes and avoid a smooth-out of the warm-core structure (Chaboureaud et al., 2012; Miglietta et al. 2011, Cavicchia 2013, Picornell et al. 2014) but may lead to an underestimation of the cyclone extension. Indeed, the radius of maximum wind is ill defined or larger during the first stage of the cyclone, but is steady and close to 90 km during the major part of its lifetime. As a result, the diagram obtained is likely less representative of the cyclone structure during its first hours but suits well from 10:00 UTC. Please note that the radius of maximum wind is ill defined or larger during the first stage of development of the cyclone, whereas it is steady and close to 90 km during the major part of its lifetime. As a result, the diagram obtained is probably not representative of the cyclone structure during its first hours.

At 06:00 UTC on 07 November, the PV streamer has moved northwards from Libya and is located south of the SLP minimum (Fig. 5a). A south-north cold front is clearly visible in the 850 hPa  $\theta_e$ , east of the cyclone centre, and the medicane centre is located under the left exit of the upper-level jet (Fig. 5b). The minimum SLP starts to decrease to reach 985 hPa around 11:00 UTC, corresponding to a strong deepening rate of 1.4 hPa hr<sup>-1</sup> for 10 hours. This phase corresponds also marks the increase of the maximum wind at low level, and of the wind speed averaged over a 100 km radius around the cyclone centre (Fig. 4). It is referred to as “development phase” in the following. The heaviest rainfall occurs here (Fig. 7) with 10 h accumulated rain above 200 mm locally and instantaneous values above 50 mm h<sup>-1</sup> east of Sicily and at sea between Pantelleria and Malta. As in Fita and Flaounas (2018), it also corresponds to the maximum thermal wind is obtained during this phase (Fig. 6).

Then, the upper-level jet then moves further over the Ionian Sea and Sicily. It and the SLP minimum is aligned with the 300 hPa PV anomaly at 11:00 UTC on 7 November (Fig. 5c). This marks the beginning of the “mature phase”, with a maximum intensity of the medicane around 12:00 UTC (Fig. 4). The medicane presents the circular shape typical of tropical cyclones with spiral rainbands, and a warm, symmetric core (Fig. 5d) extended up to 400 hPa (Fig. 6). The upper-level PV anomaly stays wrapped around the SLP until 17:00 UTC, and both structures drift eastwards south of Italy (Fig. 5e). The medicane slowly decreases in intensity (Fig. 4) until it makes landfall in the southeast of Sicily at 18:00 UTC. The cold front drifts eastwards away of the cyclone centre, evolving eventually into an occluded front (Fig. 5f) wrapped around the SLP minimum (Fig. 5f). This mature phase, although the most intense of the cyclone, produces results in more scattered rainfall than the development phase (Fig. 7).

The cyclone then moves northeastwards towards the Ionian Sea and continuously weakens until 12:00 UTC on 8 November (“decay phase” hereafter). The SLP minimum steadily increases (Fig. 4), the upper-level PV anomaly has evolved into a cut-off and is still aligned with the cyclone centre (Fig. 5g). The 850 hPa warm core has extended ~250 km around the cyclone centre (Fig. 5h).

In the following, the possible impact of the ocean-atmosphere coupling on the cyclone intensity is assessed by comparing the results of the CPL, NOCUR, and NOCPL simulations. The time period for this comparison is the 7 November only, as the medicane has lost a large part of its intensity in the evening of the 7 November.

### 3.2 SST evolution

Taking into account the effect of the SST change only (NOCUR) results in a slightly slower and weaker deepening by 1.5 hPa and almost no change of the maximum wind speed 3 m s<sup>-1</sup> higher (Fig. 4). Including the effect of the surface currents on the atmospheric boundary layer gives results in a slightly more intense cyclone (1.5 hPa less difference) at its maximum and 8 m s<sup>-1</sup> stronger maximum wind. Figure 3 shows also that no significant difference on the track is obtained between the NOCPL, NOCUR and CPL simulations, except maybe when the cyclone

centre loops east of Sicily at the end of the day. The median values of the SST difference between the CPL and NOCPL simulations over the whole domain, and the values of the 5 %, 25 %, 75 % and 95 % quantiles are shown in Figure 8. The median surface cooling is very weak ~~and reaches barely~~ (0.1 °C at the end of the development phase, ~~and is close to~~ 0.2 °C at the beginning of the decay phase). Its ~~further~~ evolution, during the decay phase, is ~~also~~ very weak with values of 0.25 °C at 23:00 UTC, on 07 November. The maximum cooling is 0.6 °C. To focus on the effects of this surface cooling on the surface processes feeding the cyclone, we used a conditional sampling technique to isolate the areas with enthalpy flux above 600 W m<sup>-2</sup> (~~this~~ corresponds to the mean value of the 80 % quantile of the enthalpy flux on the day of the 7 November). The enthalpy flux is defined here as the sum of latent heat flux  $LE$  and the sensible heat flux  $H$ . On this area (EF600 hereafter), the SST difference and its time evolution are slightly larger with a median difference of -0.2 °C at the beginning of the mature phase and ~~close to~~ -0.4 °C at the end of 7 November. In NOCUR, the SST difference obtained in NOCUR on EF600 is slightly larger than in CPL but the difference is not significant. The SST cooling on this area of highest fluxes that are responsible for supplying the mediane in heat and moisture is therefore ~~less than~~ 0.4 °C in (median value). ~~is~~ much weaker than typical cooling values observed under tropical cyclones, that commonly reach 3 to 4 °C (e.g. Black and Dickey, 2008). In addition, the spatial extent of the cooling does not ~~form~~ ~~ac~~respond to a clear wake as in tropical cyclones (not shown).

The conclusion of this part is that surface cooling ~~under this mediane~~ is one order of magnitude smaller than what is obtained under tropical cyclone, with no significant impact of the surface currents. But, quantifying the surface cooling ~~in~~ other medicanes could lead to contrasting results. For instance, ~~in an ocean-atmosphere-waves coupled simulation of a strong storm in the Gulf of Lion~~, a surface cooling of 2 °C was obtained ~~in an ocean-atmosphere-waves coupled simulation of a strong storm in the Gulf of Lion~~ (Renault et al., 2012). ~~Investigating the reasons of s~~Such a discrepancy ~~with a storm of comparable intensity cannot be explained easily, and this is~~ are beyond the scope of the present work. ~~The stronger cooling~~A possible explanation could be ~~due to~~ the storm track ~~staying at~~ affecting the same place ~~by making a loop~~ in the Gulf of Lion ~~for a long time, resulting in a larger cooling~~. The difference can also come from a different oceanic preconditioning (their case occurred in May), with stronger stratification or a shallower mixed layer ~~in the Gulf of Lion~~ that amplifies cooling due to mixing/entrainment process.

### 3.3 Impact on turbulent surface exchanges

A comparison of the time evolution of the ~~turbulent enthalpy flux, sensible and latent heat~~ fluxes in of the NOCPL and CPL simulations shows ~~very weak~~ that the differences ~~are very weak~~ even on the EF600 area (Fig. 9a). ~~At the end of the run~~During the decay phase where it is maximum, the mean difference of the enthalpy flux is 25 W m<sup>-2</sup>, with a standard deviation of 13 W m<sup>-2</sup>. ~~This is weak~~ Compared to the values of the turbulent fluxes on this area, between 500 and 800 W m<sup>-2</sup> for  $LE$  and 100 and 250 W m<sup>-2</sup> for  $H$ , ~~this value is weak~~. Expressed in percent of the fluxes, ~~values~~, the relative difference is ~~close to~~  $\approx 2$  % at the beginning of the mature phase and ~~reaches~~ 5 % at 21:00 UTC on 7 November, ~~when the mediane has weakened~~. The ~~relative~~ difference of  $H$  is  $7 \pm 4$  W m<sup>-2</sup> ~~(relative difference)~~ the sensible heat flux varies between 4 and 10 % ~~due to the lower values of  $H$ , and the value of the difference is close to 7 W m<sup>-2</sup> with a standard deviation of 4 W m<sup>-2</sup>~~. So, coupling ~~appears to~~ have a very weak impact on the turbulent heat fluxes even in the EF600 area. Again, the effect of the surface currents (CPL versus NOCUR in Fig. 9b) is not significant.

In the following, except if otherwise specified, the results of the NOCPL simulation are used to investigate the mediane behaviour, focusing on ~~what occurred~~ the area of interest (AI in Fig. 2).



#### 4 Role of surface fluxes and mechanisms

This section investigates ~~which the role of the~~ surface parameters ~~in controlling~~ the surface heat fluxes during the different phases of the medicane, ~~among the SST, surface wind, temperature and humidity. The objective is to assess the relative role of the SST, the surface wind, and the heat and moisture in the surface layer in the surface heat transfer and its time evolution.~~

##### 575 4.1 Representation of surface fluxes and methods

In numerical atmospheric models, the turbulent heat fluxes are classically computed as a function of surface parameters using bulk formulae:

$$H = \rho c_p C_h \Delta U \Delta \theta \quad (1)$$

$$LE = \rho L_v C_e \Delta U \Delta q \quad (2)$$

580 Here,  $\rho$  is with the air density,  $c_p$  the air thermal capacity and  $L_v$  the vaporization heat constant. ~~The gradient,  $\Delta U$ ,  $\Delta \theta$  and  $\Delta q$  corresponds to~~ the wind speed at first level with respect to the sea surface,  $\Delta \theta$  is the difference between the SST and the potential temperature at first level  $\theta$ , and  $\Delta q$  is the difference between the specific humidity at saturation with temperature equal to SST and the specific humidity at first level, ~~respectively~~. The transfer coefficients  $C_h$  and  $C_e$  are defined as

$$C_h^{1/2} = \frac{C_{hn}^{1/2}}{1 - \frac{C_{hn}^{1/2}}{\kappa} \psi_T(z/L)} \quad (3)$$

585 and

$$C_e^{1/2} = \frac{C_{en}^{1/2}}{1 - \frac{C_{en}^{1/2}}{\kappa} \psi_q(z/L)} \quad (4)$$

with  $\kappa$  the von Karman's constant,  $\psi_T$  and  $\psi_q$  empirical functions describing the stability dependence,  $C_{hn}$  and  $C_{en}$  the neutral transfer coefficient for heat and moisture and  $L$  the Obukhov length (which depends, in turn, on the virtual potential temperature at first level and on the friction velocity  $u_*$ ). In the ECUME parameterization used in this study, the neutral transfer coefficients  $C_{hn}$  and  $C_{en}$  are defined as polynomial functions of the 10 m equivalent neutral wind speed (defined as in Geernaert and Katsaros, 1986).

590 ~~They also transfer coefficients~~ depends on the wind speed at 10 m and on the Obukhov length through the stability functions. The Obukhov length is expressed as in Liu et al. (1979):

$$L = -\frac{T_v^2 u_*^2}{\kappa g T_{v*}} \quad (5)$$

595 with  $T_v$  the virtual temperature at the first level, depending on the temperature and specific humidity, and  $T_{v*}$  the scale parameter for virtual temperature depending on the temperature and humidity at the first level. As a consequence, the transfer coefficients depend as the fluxes on the wind speed, on the temperature and specific humidity at the first level, and on the SST. In the following, we do not distinguish between the temperature and potential temperature at first level.

The time evolution of the median values, and 5 %, 25 %, 75 % and 95 % quantiles of the latent and sensible heat fluxes is 600 giveshown in Figure 10a for the 7 November, on the EF600 area, and the time evolution of the median values and quantiles of the SST in Figure 10b. The latent heat flux is always much higher than the sensible heat flux, as this is generally the case at sea when the SST is above 15 °C (e.g. Reale and Atlas, 2001). The sensible heat flux represents here 22 % of the ~~enthalpytotal turbulent~~ flux during the development phase, 12 to 15 % during the decay phase. Both fluxes haveshow asymmetric distributions with upper tails (95 %) longermore distant from the median than the lower tails (5 %). This is

partly due to the conditional sampling ( $LE + H > 600 \text{ W m}^{-2}$ ) used here, as low fluxes are cut off ~~by the sampling~~. The median value of  $H$  is maximum at the end of the development phase ( $180 \text{ W m}^{-2}$  at 08:00 UTC), while ~~the maximum value of~~ its 95 % quantile is ~~maximumreached~~ at the beginning of the development phase ( $332 \text{ W m}^{-2}$  at 04:00 UTC). During the mature phase, both the median and 95 % quantile values of  $H$  ~~decreaseare~~ continuously ~~decreasing~~. Conversely, ~~the maximum of~~ the median value of  $LE$  ~~is maximum~~ ( $635 \text{ W m}^{-2}$ ) ~~is reached~~ at 09:00 UTC during the development phase and ~~it~~ stays approximately constant until 15:00 UTC. ~~The maximum of~~ the 95 % quantile ~~is maximum~~ ( $845 \text{ W m}^{-2}$ ) ~~is reached~~ at the end of the development phase. ~~The decrease of~~  $LE$  starts ~~to decrease~~ later ~~and more slowly~~ than ~~the for~~  $H$  (around 15:00, as the system has started to weaken) ~~and is slower until the end of the 7 November~~. The median values of  $LE$  in this EF600 sampling are constant or slightly increasing until the evening (20:00 UTC), whereas the minimum values (5 % quantile) increase continuously until the end of the day. Again, this is probably partly due to the sampling used here.

The ~~distributiontime evolution of the median values and quantiles of the of the~~ SST ~~shows, conversely, are~~ asymmetric ~~throughout the event, distributions~~ with lower tails much longer than upper tails (Fig. 10b). The SST maximum (~~close to 24 °C~~) ~~values of SST (95 % quantile) are is~~ almost constant with time, ~~and close to 24 °C~~, while ~~t~~ the lower and median values vary due to the conditional sampling EF600 and the motion of the cyclone away from the warm SST area.

To investigate the mutual dependencies and co-variabilities of the fluxes and parameters listed above, we used the rank correlation of Spearman, which corresponds to the ~~Pearson or~~ linear correlation between the rank of the two variables in their respective sampling (Myers et al., 2010). This metrics enables relating monotonically rather than linearly the variables of interest and is more appropriate in the case of non-linear relationships, ~~as this is the case for the fluxes that may be related to the variables additionally through the transfer coefficients~~.

The co-variabilities are analysed ~~first~~ in the whole domain ~~first~~, to determine ~~the main contribution what contributes the most~~ to the fluxes globally, then in the EF600 area to isolate ~~surface~~ processes ~~controllingexplicitly responsible for the fluxes contributing the most to~~ the growth and maturity of the medicane. The ~~corresponding~~ values are given in Tables 1 to 3 for the EF600 area, and for 3 time periods ~~considered representative~~ of the development, mature and decay phases respectively, i.e. 09:00, 13:00 and 18:00 UTC on 7 November.

## 4.2 Development phase

At low level, this phase corresponds to a low-pressure system resulting ~~fromof~~ the evolution of the instability generated by the lee cyclone ~~ofinduced by~~ the North African relief, with strong baroclinic structures. ~~During the first hours, t~~ ~~The areas of~~ heavy precipitation ~~obtained during the first hours~~ are co-localized with frontal structures. A warm sector is ~~visiblepresent at~~ ~~the~~ east of the domain, with a cold front extending south-east from the south of Italy and ~~a~~ very strong low-level convergence between ~~thea~~ southeasterly flow in the warm sector and ~~thea~~ south to southwesterly flow in the cold sector (~~see~~ ~~Fig. 5b~~).

At 08:30 UTC on 7 November (Fig. 11), strong convergence lines ~~developare present~~ between Sicily and Tunisia, close to the cyclonic centre. The low-level virtual potential temperature  $\theta_v$  superimposed to the equivalent potential temperature  $\theta_{e-on}$  ~~the map (Fig. 11a) and on an east-west (E-W) cross section close to the SLP minimum (Fig. 11b)~~ is used here as a marker of cold pools (with an upper limit of  $19^\circ\text{C}$  for  $\theta_v$  – Ducrocq et al., 2008; Bresson et al., 2012). Some of these cold pools ~~are the result fromof~~ ~~evaporationng processes~~ under convective precipitation, while those located at sea along the North African coast originates from dry and cold air advected from inland. ~~(T~~ the discrimination between these two kinds of cold pools was done using a simulation without the latent heat transfer due to rain evaporation; (not shown here). The cold and moist air spreads to the surface following density currents and is advected northw~~e~~astwards by the low-level flow. On the west and south of the domain, cold pools were

formed at night by radiative processes over land, ~~and then were~~ advected over sea with a vertical extent of  $\sim 1000$  m (see the westernmost part of the W-E transect, Fig. 11b).

The upwind edge of the cold pools is the place of the strong horizontal convergence at low level, leading to uplift and deep convection on air masses with high  $\theta_e$ , ~~is located on the upwind edge of the cold pools~~. During this development phase, the cold pools ~~located in the southerly flow~~ move northwards ~~with the southerly flow~~, towards the centre of the cyclone. ~~Then, they contribute to and trigger~~ convection up to 3000 m of the northwesterly low-level flow with high  $\theta_e$  (Fig. 11b). ~~This propagates~~ the surface warm anomaly ~~propagates~~ close to the cyclone centre (now located under the 300 hPa PV anomaly) up to 3000 m and ~~generates/develops a corresponding~~ low- to mid-troposphere PV anomaly. At the same time, a dry air intrusion from the upper levels brings air masses with low  $\theta_e$  and relative humidity below 20 % to 3000 m, resulting in a upper-to-mid-troposphere PV anomaly (Fig. 15a and c).

To identify the surface parameters controlling evaporation at sea, the time evolution of the Spearman's rank correlations between ~~LE the latent heat flux~~,  $U_{10}$ ,  $\theta$ , the SST and  $q$  is given in Figure 12 and Tables 1 to 3.

During this phase, on the whole domain, the ~~controlling~~ parameters ~~governing for~~  $LE$  are the SST and the wind (positively correlated), the specific humidity (negatively) and the potential temperature (negatively). Potential temperature and humidity are also strongly positively correlated ( $r_s = 0.55$  over the whole domain), ~~because due to the advection of cold and dry air is advected from the Tunisian and Libyan continental surface~~ by the southerly low-level flow ~~from the Tunisian and Libyan continental surface~~ (Fig. 13b, c and f, at 09:00 UTC). This air mass progressively charges itself in heat and moisture on the area of strongest enthalpy fluxes at sea north of the Libyan coasts (Fig. 13a). The EF600 area, ~~with of~~ strong fluxes and cold/dry air, corresponds also to ~~the area of~~ warm SSTs (Fig. 13e). ~~Here, Within this area, the main influence on LE is mainly controlled by from the wind and by, then from the SST (Fig. 12b, Table 1). There is no effect of the potential temperature  $\theta$  has no effect (weak or negative correlations, Fig. 12b, Table 1), and a weak effect of the specific humidity  $q$  a weak effect.~~

$LE$  is always much higher than  $H$  (Fig. 10a), resulting in the “strong flux area” EF600 ~~being determin being controlled by LE values rather than  $H$  values, and LE is also more homogeneous values of LE than  $H$  on EF600 over this area.~~ However,  $H$  can ~~reach~~ strong values locally ~~with respect to the LE during this development phase. As a consequence, values of  $H$  still show strong contrast on the EF600 area~~ (Fig. 13d). During this development phase,  $H$  is controlled mainly by the potential temperature  $\theta$  at first level (Fig. 14), partly indirectly through the stratification and transfer coefficient (not shown). On the EF600 area also,  ~~$H$  is mainly governed by  $\theta$  the SST influence is weak at all times, the major control is also from the potential temperature ( $r_s = -0.70$  at 09:00 UTC), the SST influence is always weak.~~ The wind plays a secondary role. The enhanced control by the potential temperature is partly due to the continental air masses advected from North Africa, and partly to the presence of the cold pools under the areas of deep convection and strong wind. ~~The  $H$  values are located offshore of the Tunisian and Libya coasts downwind of the strong low-level flow bringing cold air from the continent.~~

### 4.3 Mature phase

At 13:00 on 7 November, the PV anomalies at 700 hPa and 300 hPa are aligned (Fig. 15c, e). A zonal cross section on the SLP minimum shows that a low-level PV anomaly ~~with values~~ above 5 PVU has formed around the ~~centre of~~ cyclone centre, extending from the surface up to the 300 hPa anomaly (Fig. 15). The warm core ~~of the systems~~ extends up to 850 hPa (Fig. 15a), ~~its upward development is and is~~ limited ~~upward~~ by colder air (low  $\theta_e$ ) brought from aloft. ~~The re is tangential velocity field shows~~ low-level convergence (up to 800 hPa) towards the cyclone centre, deep convection close to the centre, but no or very weak divergence at mid to upper troposphere. The cyclonic circulation has reinforced with horizontal wind speed above  $8 \text{ m s}^{-1}$  at ~~every level all heights out of a radius of more than~~ 10 km ~~away from around~~ the cyclone centre.

During this phase ~~ands~~ the previous one, over the whole domain as in the EF600 area, ~~the dominant role in controlling~~ evaporation is ~~controlled~~~~played~~ equivalently by the SST ~~and with an effect equivalent to~~ the wind speed, ~~with~~ a decreasing influence of the humidity (Fig. 12, Table 2). The ~~area~~ EF600 area extends further north, closer to the cyclone centre, away from the area of cold and dry low-level air. ~~This cold air inflow, starts to which also tends to~~ warm and moisten under the combined impact of the diurnal warming of the continental surfaces (not shown) and of the strong enthalpy fluxes offshore (Fig. 16a, c and f). The sensible heat flux is still controlled by the temperature, with an increasing influence of the wind (Table 2).

#### 4.4 Decay phase

In the afternoon of the 7 November, the cyclone first moves towards colder SSTs in the east of the Sicily Strait (Fig. 3). ~~Then, it~~ crosses Sicily and reaches es the Ionian Sea with even colder SSTs around 20:00 UTC, ~~with even colder SSTs~~, before slowly decaying and losing its tropical-like characteristics. ~~Backtrajectories were used to check to role played by whether~~ warm and moist air extraction from the sea-surface contributes to high  $\theta_e$  values obtained around the cyclone centre, in ~~feeding the cyclone centre by air masses with high  $\theta_e$  values, backtrajectories were used starting~~ They at 23:00 on the 7 ~~November, south of the cyclone centre use the method of~~ (Schär and Wernli, (1993) ~~adapted by~~; Gheusi and Stein, (2005). The chosen trajectories ~~of three air parcels~~ originating from three every different places and arriving at the same place, at three vertical levels surrounding the level closest to 1500 m, at 23:00 on the 7 November are shown in (Fig. 17). Their equivalent potential temperature ranges from 31 to 38 °C at their first appearance in the domain and is close to 45 °C on average ~~at when they reach~~ their final point. On the ~~seir~~ trajectories,  $\theta_e$  increases almost continuously, with a strong jump during their transit at low level (below 500 m) above ~~the~~ sea in the EF600 area (white contour in Fig. 17). A separate analysis of the two different stages ~~in of~~ the trajectories has been performed. Stage 1 corresponds to the period when the particles remain in the low-level flow (between 200 and 1200 m above sea level) south and east of Sicily and stage 2 to their convective ascent from ~ 300 m to 1500 m. During stage 1, the potential temperature of the particles decreases of 1 °C in average while the mixing ratio increases of 2.8 g kg<sup>-1</sup>. This shows that the increase in  $\theta_e$  is due to strong surface evaporation. During stage 2, the mixed ratio of the particles decreases of 2 g kg<sup>-1</sup> and their potential temperature increases of 4.1 °C. This indicates condensation and latent heating. This demonstrates the strong role of the sea surface in increasing the moisture and heat of the low-level flow before its approach of the cyclone centre, and of diabatic processes in reinforcing its warm core.

During the decay phase and in the whole domain; the influence of the humidity on LE ~~the evaporation, in the whole domain~~ is weak (Fig. 12a). ~~EF600 The area of strong enthalpy fluxes~~ is still located on warm SSTs, ~~on the~~ south of the domain (Fig. 18a, e), and corresponds also to which is also the place of the strongest winds on the right-hand side of the cyclone (Fig. 18b). Within this ~~EF600~~ area, there is almost no influence of the temperature or humidity on *LE* (Table 3). The influence of the wind speed is decreasing; ~~the~~ role of the SST is strong until 21:00 UTC. ~~After that, when~~ the cyclone reaches the northern Ionian Sea ~~with here the SST is~~ much colder SSTs, and the effect of the wind speed becomes dominant at the very end (Fig. 12b). ~~Concerning the sensible heat flux, there are less patches of strong flux corresponding to cold pools and low  $\theta$ , but a is~~ governed by the wind (see the strong NS gradient in Fig. 18b) rather than by the low-level temperature, except in the northern part of EF600 (where the wind speed is also the highest). medium-scale northwest-southeast gradient of  $H$  over the EF600 area, related to a NS gradient of wind speed (Fig. 18b). On the north of the EF600 area (where the wind speed is also the highest), the potential temperature is colder and  $H$  values are maximum.

In summary, at the scale of the domain, ~~the latent heat flux (evaporation) is controlled by the SST and wind throughout the day of the 7 November~~: both strong winds (in the cold sector during the development phase, then close to the cyclone centre and in its right side) and warm SSTs (in the south of the domain) are ~~thus~~ necessary to ~~have~~ strong latent heat fluxes. Within

the area ~~of strong where the turbulent~~ fluxes ~~are high~~ (also ~~nd where strong winds are strong~~ and ~~warm~~ SSTs ~~high~~), the ~~control of~~ evaporation is mainly ~~controlled by from~~ the wind (development and mature phases) then ~~by from~~ the SST (decay phase). In contrast, the sensible heat flux ~~dependis always~~ mainly ~~on controlled by~~ the potential temperature in the surface layer. Colder air masses ~~lead to result in enhanced strong~~ sensible heat flux, rather than strong wind or warmer SST. During the two first phases, ~~this~~ cold air is either advected from North Africa or created by evaporation under convective precipitation (cold pools). During the decay phase, strong latent heat transfer over ~~high warm~~ SSTs warms the near-surface atmospheric layer and ~~results finally in~~ lowers ~~the~~ sensible heat transfer.

## 5 Discussion and conclusion

The comparison of the simulations with and without ocean coupling shows no significant impact of the evolution of the SST on the track, intensity or lifecycle of the medicane. The weak SST cooling, notably during the first 24 h of the simulation, is likely responsible for that. On the strong flux area, where the enthalpy flux feed~~ings~~ the cyclone in heat and moisture maintain~~ing~~ the convection and the latent heat release ~~mechanism~~, the median value of the SST cooling is ~~between~~ 0.2°C ~~during the mature phase~~, and ~~reaches barely~~ 0.4 °C ~~at the end of the day~~. The ~~effect median difference~~ on  $H$  is  $-7 \text{ W m}^{-2}$  during the mature phase,  $-12 \text{ W m}^{-2}$  at 23:00 UTC on the 7 November (~~representing less than 10 % difference~~). ~~On LE, it is;~~ and  $-19 \text{ W m}^{-2}$ , ~~and~~  $-37 \text{ W m}^{-2}$  ~~on LE at for~~ the same two time periods (~~representing less than 5 % difference~~). Coupling with the surface currents has no significant impact of the simulation.

~~NThe co-variabilities of surface fluxes and parameters show nevertheless that~~, in this specific case, the SST exerts a strong control on the latent heat flux that dominates the surface heat transfer, throughout ~~the whole duration of~~ the event. During ~~theits~~ development phase, there is also a strong influence of peculiarities of the Central Mediterranean: the transition between deep convection and heavy precipitation associated with baroclinic processes and the ~~tropical-like~~ cyclone tak~~ing~~s place downwind of the ~~dry and cold~~ low-level flow ~~of dry and cold air originated~~ from North Africa. These air masses with low  $\theta$ , encounter moist and warm air ~~resulting of the strong sea surface evaporational at sea~~ and enhance the deep convection ~~at sea~~, together with the cold pools formed by rain evaporation and downdrafts. These cold pools of various origin~~s~~ displace the deep convection at sea. Uplift of warm air masses increases the low-level PV, and reinforces the vortex, which is moved northeastwards closer to the PV anomaly aloft.

~~It has recently been suggested that medicanes could be sorted into two (possibly three) different categories according to the intensity and role of air-sea heat exchanges and to the related surface mechanisms (Miglietta and Rotunno, 2019). The main difference between these two categories is the processes leading to the warm core of the cyclone. The first category corresponds to purely WISHE-like mechanisms, with latent heat release fed by heat and moisture extracted from the sea surface as processes responsible for the medicane deepening and warm-core building. The cyclone is detached from any large-scale, baroclinic structure during its mature phase, with no transfer of PV from the upper-level jet. The PV anomaly at all levels consists in: wet potential vorticity (WPV) produced diabatically by latent heat release (Eq. 4 in Miglietta et al., 2017) and dry potential vorticity (DPV) brought by intrusion of stratospheric air into the upper troposphere (their Eq. 3). Levels up to  $\sim 600$  hPa present a maximum of WPV due to latent heating, while DPV is almost constant up to  $\sim 400$  hPa where it increases sharply, and there is no real PV tower around the cyclone centre. The features characteristics of tropical cyclones are well marked: warm core extending up to 800 hPa, symmetry, low-level convergence and upper-level divergence, and strong contrast of  $\theta_e$  ( $\sim 8$  °C) between the surface and 900 hPa as an evidence of latent heating. The case of October 1996 chosen to represent this category shows very strong surface fluxes (above  $1500 \text{ W m}^{-2}$  over large areas) due to strong, persistent winds of orographic origin bringing cold and dry air for several days prior to the cyclone development, also contributing to destabilize the surface layer.~~



Medicanes of the second category also present similarities with tropical cyclones, like deep warm core and symmetrical wind field, but present both diabatic and baroclinic processes throughout their lifetime. The cyclone stays within a large-scale baroclinic environment, with the PV streamer slowly evolving into a cut-off low. The tropical-like features are less evident: weaker warm core, weaker gradient of  $\theta_e$  ( $\sim 3-4^\circ\text{C}$ ) between the surface and 900 hPa. Around the cyclone centre, a PV tower forms, with weak contrast between the DPV and WPV profiles. As an example, the warm core of the December 2005 medicane is not due to convective latent heating but to seclusion of warm air by colder air masses and extends up to 400 hPa. The surface enthalpy fluxes play only a marginal role and take maximum values of  $1000\text{ W m}^{-2}$  for a few hours.

Better knowing the intensity and the role of air-sea exchanges and the related mechanisms could permit to sort medicanes, as proposed by Miglietta and Rotunno (2019). Indeed, is the present case governed by WISHE-like mechanisms or rather by diabatic and baroclinic processes throughout its lifetime (second category in Miglietta and Rotunno, 2019)? In the present case of Qendresa, strong air-sea exchanges at the surface and latent heat release act at building the warm core anomaly, as seen in Sect. 4.3 and 4.4. The surface enthalpy fluxes take intermediate values with maximum above  $1500\text{ W m}^{-2}$  for a few hours on areas with warm SST and strong winds downwind of the dry low-level flow from North Africa. Thermal features characteristic of tropical cyclones are present, like low-level cold air advection from the south to the east, and warm air advection from the south to the north (Reale and Atlas, 2001), and the gradient of  $\theta_e$  between the surface and 900 hPa is around intermediate values of  $6-7^\circ\text{C}$ . The wrapping of the PV streamer around the cyclone centre evolves into an upper-level cut-off at the end of the decay phase. Conversely, some typical features are not present: even if there is weak low-level convergence around the cyclone centre, no divergence is seen obtained at upper level. The area of maximum latent heat flux within the EF600 area is more controlled by the SST than by the wind speed (Fig. 12b and 13a, b, and e). No minimum of potential temperature or potential vorticity develop at 300 hPa close to the cyclone centre during the mature phase, as a marker of the PV anomaly erosion by the convective activity, and the upper-level PV anomaly never completely detaches from the large scale structure.

Figure 19 shows the vertical profiles of wet PV and dry PV (WPV and DPV, defined as in Miglietta et al., 2017) averaged on the 100 km radius circle around the cyclone centre. WPV is produced diabatically by latent heat release (their Eq. 4) and DPV is generated by intrusion of stratospheric air into the upper troposphere (their Eq. 3). The vertical profiles of PV, DPV and WPV (defined as in Miglietta et al., (2017)) averaged on a 100 km radius circle around the cyclone centre show a minimum of WPV between 700 and 400 hPa during the decay phase, and a clear difference between DPV and WPV at low level (Fig. 19). The DPV is weak up to the mid troposphere and increases sharply above 400 hPa. The WPV anomaly at low levels that develops up to 700 hPa during the development phase is increased but its vertical extent is reduced to 800 hPa during the mature phase (13:00 UTC – see also Fig. 15e). This is due to a dry air intrusion during the mature and decay phases, which is limited downwards by to mid-troposphere because of the warm core (Fig. 15a). At the beginning of the decay phase, at 18:00 UTC, the latent heating within the cyclone core increases the low-level WPV at low level and erodes the dry and cold ( $\theta_e$ ) air masses up to 650 hPa. The warm core and WPV anomaly extend upwards (Fig 15b, f), and the DPV anomaly is pushed up to 700 hPa (Fig. 15c, d).

This suggests that the medicane of November 2014 as simulated in this study presents characteristics close to an extratropical cyclone, or medicane of the second category as in Miglietta and Rotunno (2019). Its development phase is triggered by a PV streamer bringing instability at upper level, and baroclinic processes followed by strong convection at sea. This convection is enhanced and maintained by cold pools due to rain evaporation at low level or by advection of dry and cold air from North Africa. The conjunction of advection of continental air masses with evaporation under storms has not been identified as leading to tropical transition of Mediterranean cyclones so far, even though it is probably rather ubiquitous. Indeed, as both phenomena are rather widespread phenomena in the Mediterranean. Surface fluxes are strong and

contribute to enhance the convection potential till the mature phase of the cyclone. Evaporation is mainly controlled by the SST and by the wind speed during the whole event, while the temperature difference between the SST and the cold air advected from North Africa during the development and mature phase play a strong role during its development. The vertical development of the warm core is limited, ~~at the beginning of the decay phase,~~ by a dry air intrusion that does not reach the lowest levels of the troposphere. Dry air intrusions have been recognized as common processes in Mediterranean cyclones by Flaounas et al. (2015) but their role in the cyclone lifecycle was not clearly assessed. Here, we suggest that they can act at limiting the extent of the convection at the beginning of the mature phase. The convective activity is stronger during the development than during the mature phase of the cyclone, resulting in heavy rainfall 12 to 6 h before the maximum wind speed, in consistency with previous studies ~~of medicanes~~-based on observations (Miglietta et al., 2013; Dafis et al., 2018). Finally, these results are consistent with those of Carrió et al. (2017), ~~which show~~By using a factor separation technique, ~~they show~~ that while the role of the upper-level PV anomaly is crucial in preconditioning the event, its rapid deepening is due to the synergy of latent heat release and upper-level dynamics.

Coupling the atmospheric model with a 3D high-resolution oceanic model shows that, ~~in the present case,~~ the surface cooling ~~susceptible to affect the surface fluxes~~ is too weak ~~in that case~~ to impact the atmospheric destabilization processes at low level. Nevertheless, the effect of the medicane on the oceanic surface layer is probably significant. To better understand the sea surface evolution and the role of coupling, the ocean mixed layer response to the medicane and the mechanisms involved will be investigated in more details in future work.

**Author contributions.** MNB and CLB designed the simulations. MNB performed the simulations. Both authors interpreted the results and wrote the paper.

**Competing interests.** The author declare that they have no conflict of interest.

## Acknowledgments

This work is a contribution to the HyMeX program (Hydrological cycle in the Mediterranean EXperiment - <http://www.hymex.org>) through INSU-MISTRALS support. The authors acknowledge the Pôle de Calcul et de Données Marines for the DATARMOR facilities (storage, data access, computational resources). The authors acknowledge the MISTRALS/HyMeX database teams (ESPRI/IPSL and SEDOO/OMP) for their help in accessing to the surface weather station data. The PSY2V4R4 daily analyses were made available by the Copernicus Marine Environment Monitoring Service (<http://marine.copernicus.eu>). The ERA5 reanalysis at hourly timescales (doi: 10.24381/cds.bd0915c6) are produced by the European Centre for Medium-Range Weather Forecasts (ECMWF) and made available by the Copernicus Climate Change Service (<https://cds.climate.copernicus.eu>). METAR observations of SLP and wind were retrieved through the Weather Wunderground portal <https://www.wunderground.com>. The authors thank J.-L. Redelsperger (LOPS) for valuable discussions. We also thank E. Flaounas and an anonymous reviewer whose comments helped to greatly improve this paper.

## References

Akhtar, N., Brauch, J., Dobler, A., Béranger, K. and Ahrens, B.: Medicanes in an ocean–atmosphere coupled regional climate model, *Nat. Hazards Earth Syst. Sci*, 14, 2189–2201, 2014.

- 840 Arsouze, T., Beuvier, J., Béranger, K., Somot, S., Lebeaupin Brossier, C., Bourdallé-Badie, R., Sevault, F., and Drillet, Y.: Sensibility analysis of the Western Mediterranean Transition inferred by four companion simulations, The Mediterranean Science Commission, Monaco, in Proceedings of the 40th CIESM Congress, November 2013, Marseille, France, 2013.
- Barnier, B., Madec, G., Penduff, T., Molines, J.-M., Treguier, A.-M., Le Sommer, J., Beckmann, A., Biastoch, A., Böning, C., Dengg, J., Derval, C., Durand, E., Gulev, S., Remy, E., Talandier, C., Theetten, S., Maltrud, M., McClean, J., and De  
845 Cuevas, B.: Impact of partial steps and momentum advection schemes in a global ocean circulation model at eddy-permitting resolution. *Ocean Dyn.* 56 (5), 543–567, <https://doi.org/10.1007/s10236-006-0082-1>, 2006.
- Belamari, S.: Report on uncertainty estimates of an optimal bulk formulation for surface turbulent fluxes, Marine EnviRonment and Security for the European Area–Integrated Project (MERSEA IP), Deliverable D, 4, 2005.
- Belamari, S. and Pirani, A.: Validation of the optimal heat and momentum fluxes using the ORCA2-LIM global ocean-ice  
850 model, Marine EnviRonment and Security for the European Area–Integrated Project (MERSEA IP), Deliverable D, 4, 2007.
- Beuvier, J., Béranger, K., Lebeaupin Brossier, C., Somot, S., Sevault, F., Drillet, Y., Bourdallé-Badie, R., Ferry, N., and Lyard, F.: Spreading of the Western Mediterranean deep water after winter 2005: time scales and deep cyclone transport, *J. Geophys. Res.: Oceans* 117 (C7), <https://doi.org/10.1029/2011JC007679>. C07022, 2012.
- 855 Black, W. J., and Dickey, T.D.: Observations and analyses of upper ocean responses to tropical storms and hurricanes in the vicinity of Bermuda, *J. Geophys. Res.*, 113, C08009, doi:10.1029/2007JC004358, 2008.
- Blanke, B., and Delecluse, P.: Variability of the tropical Atlantic Ocean simulated by a general circulation model with two different mixed-layer physics. *J. Phys. Oceanogr.* 23 (7), 1363–1388. <https://doi.org/10.1175/1520-0485023<1363:VOTTAO>2.0.CO;2>, 1993.
- 860 Bougeault, P. and Lacarrère, P.: Parameterization of Orography-Induced Turbulence in a Mesobeta-Scale Model. *Mon. Weather Rev.*, 117, 1872–1890. [https://doi.org/10.1175/1520-0493\(1989\)117<1872:POOITI>2.0.CO;2](https://doi.org/10.1175/1520-0493(1989)117<1872:POOITI>2.0.CO;2), 1989.
- Bresson, E., Ducrocq, V., Nuissier, O., Ricard, D., and de Saint-Aubin, C.: Idealized numerical study of southern France heavy precipitating events: Identification of favouring ingredients. *Q. J. R. Meteorol. Soc.*, 138: 1751–1763, 2012.
- Carrió, D. S., Homar, V., Jansà, A., Romero, R. and Picornell, M. A.: Tropicalization process of the 7 November 2014  
865 Mediterranean cyclone: numerical sensitivity study, *Atmospheric Research*, 197, 300–312, 2017.
- [Cavicchia, L. and Gualdi, S.: A long-term climatology of medicanes. \*Climate Dyn.\*, 43, 1183–1195, doi:10.1007/s00382-013-1893-7, 2014.](#)
- Chaboureaud, J.-P., Pantillon, F., Lambert, D., Richard, E. and Claud, C.: Tropical transition of a Mediterranean storm by jet crossing, *Q. J. Roy. Meteorol. Soc.*, 138, 596–611, 2012.
- 870 Cioni, G., Cerrai D., and Klocke D.: Investigating the predictability of a Mediterranean tropical-like cyclone using a storm-resolving model, *Q. J. Roy. Met. Soc.*, 144, 1598–1610, doi: 10.1102/qj.3322, 2018.
- [Claud, C., Alhammoud, B., Funatsu, B. M., and Chaboureaud, J. P.: Mediterranean hurricanes: large-scale environment and convective and precipitating areas from satellite microwave observations. \*Nat. Hazards Earth Syst. Sci.\*, 10\(10\), 2199, 2010.](#)
- 875 Colella, P. and Woodward, P.R.: The Piecewise Parabolic Method (PPM) for Gas-Dynamical Simulations. *Journal of Computational Physics*, 54, 174–201, [https://doi.org/10.1016/0021-9991\(84\)90143-8](https://doi.org/10.1016/0021-9991(84)90143-8), 1984.
- Cuxart, J., Bougeault, P. and Redelsperger, J.L.: A turbulence scheme allowing for mesoscale and large-eddy simulations, *Q. J. Roy. Meteorol. Soc.*, 126, 1–30. <https://doi.org/10.1002/qj.49712656202>, 2000.



- D'Asaro, E. A., Sanford, T. B., Niiler, P. P., and Terrill, E.J.: Cold wake of Hurricane Frances. *Geophys. Res. Lett.*, 34, L15609, doi:10.1029/2007GL030160, 2007.
- Dafis, S., Rysman, J. F., Claud, C., and Flaounas, E.: Remote sensing of deep convection within a tropical-like cyclone over the Mediterranean Sea. *Atmospheric Science Letters*, 19(6), e823, 2018.
- [Davolio S, Miglietta MM, Moscatello A, Pacifico F, Buzzi A, and Rotunno R.: Numerical forecast and analysis of a tropical-like cyclone in the Ionian Sea. \*Nat. Hazards Earth Syst. Sci.\* 9: 551–562, 2009.](#)
- Di Muzio, E., Riemer, M., Fink, A. H., and Maier-Gerber, M.: Assessing the predictability of Medicanes in ECMWF ensemble forecasts using an object-based approach. *Q. J. R. Meteorol. Soc.*, 145(720), 1202–1217, 2019.
- Ducrocq, V., Nuissier, O., and Ricard, D.: A numerical study of three catastrophic precipitating events over southern France. Part II: Mesoscale triggering and stationarity factors. *Q. J. R. Meteorol. Soc.* 134: 131–145, doi.org/10.1002/qj.199, 2008.
- Emanuel, K.A.: An air–sea interaction theory for tropical cyclones. Part I: Steady-state maintenance, *J. Atmos. Sci.*, 43, 585–604, 1986.
- Fita, L., and Flaounas, E.: Medicanes as subtropical cyclones: the December 2005 case from the perspective of surface pressure tendency diagnostics and atmospheric water budget, *Q. J. Roy. Meteorol. Soc.*, 144, 1028–1044, doi: 10.1002/qj.3273, 2018.
- Flaounas, E., Raveh-Rubin, S., Wernli, H., Drobinski, P. and Bastin, S.: The dynamical structure of intense Mediterranean cyclones, *Clim. Dynam.*, 44, 2411–2427, doi: 10.1007/s00382-014-2330-2, 2015.
- Flaounas, E., et al.: Assessment of an ensemble of ocean–atmosphere coupled and uncoupled regional climate models to reproduce the climatology of Mediterranean cyclones. *Clim. Dynam.*, 51(3), 1023–1040, 2018
- [Gaertner, M. A., Jacob, D., Gil, V., Domínguez, M., Padorno, E., Sánchez, E., and Castro, M.: Tropical cyclones over the Mediterranean Sea in climate change simulations. \*Geophys. Res. Lett.\*, 34\(14\), 2007.](#)
- Gaertner, M.A., Gonzalez-Aleman, J.J., Romera, R., Dominguez, M., Gil, V., Sanchez, E., Gallardo, C., Miglietta, M.M., Walsh, K., Sein, D., Somot, S., dell'Aquila, A., Teichmann, C., Ahrens, B., Buonomo, E., Colette, A., Bastin, S., van Meijgaard, E. and Nikulin, G.: Simulation of medicanes over the Mediterranean Sea in a regional climate model ensemble: impact of ocean-atmosphere coupling and increased resolution, *Clim. Dynam.*, 51, 1041–1057, 2017.
- [Geernaert, G., and Katsaros, K. B.: Incorporation of stratification effects on the oceanic roughness length in the derivation of the neutral drag coefficient. \*J. Phys. Oceanogr.\*, 16\(9\), 1580–1584, 1986.](#)
- Gheusi, F., and Stein, J.: Lagrangian trajectory and air-mass tracking analyses with Meso-NH by means of Eulerian passive tracers, *Techn. Doc.*, [http://mesonh.aero.obs-mip.fr/mesonh/dir\\_doc/lag\\_m46\\_22avril2005/lagrangian46.pdf](http://mesonh.aero.obs-mip.fr/mesonh/dir_doc/lag_m46_22avril2005/lagrangian46.pdf), accessed on 18/02/2019, 2005.
- Hart, R.E.: A cyclone phase space derived from thermal wind and thermal asymmetry, *Mon. Weather Rev.*, 131, 585–616, 2003.
- Homar, V., Romero, R., Stensrud, D.J., Ramis, C. and Alonso, S.: Numerical diagnosis of a small, quasi-tropical cyclone over the western Mediterranean: dynamical vs. boundary factors, *Q. J. Roy. Meteorol. Soc.*, 129, 1469–1490, 2003.
- Lac, C., Chaboureaud, J.-P., Masson, V., et al.: Overview of the Meso-NH model version 5.4 and its applications, *Geosci. Model Dev.*, 1, 1929–1969, <https://doi.org/10.5194/gmd-11-1929-2018>, 2018.

- Lazar, A., Madec, G., and Delecluse, P.: The deep interior downwelling, the Veronis effect, and mesoscale tracer transport parameterizations in an OGCM. *J. Phys. Oceanogr.* 29 (11), 2945–2961. [https://doi.org/10.1175/1520-0485\(1999\)029<2945:TDIDTV>2.0.CO;2](https://doi.org/10.1175/1520-0485(1999)029<2945:TDIDTV>2.0.CO;2), 1999.
- Lebeaupin Brossier, C., Arsouze, T., Béranger, K., Bouin, M.-N., Bresson, E., Ducrocq, V., Giordani, H., Nuret, M.,  
920 Rainaud, R., and Taupier-Letage, I.: Ocean Mixed Layer responses to intense meteorological events during HyMeX-SOP1 from a high-resolution ocean simulation, *Ocean Model.*, 84, 84–103. <https://doi.org/10.1016/j.ocemod.2014.09.009>, 2014.
- Lellouche, J.-M., Le Galloudec, O., Drévillon, M., Régnier, C., Greiner, E., Garric, G., Ferry, N., Desportes, C., Testut, C.-E., Bricaud, C., Bourdallé-Badie, R., Tranchant, B., Benkiran, M., Drillet, Y., Daudin, A., and De Nicola, C.: Evaluation  
925 of global monitoring and forecasting systems at Mercator Océan, *Ocean Sci.*, 9, 57–81, <https://doi.org/10.5194/os-9-57-2013>, 2013.
- Liu, W. T., Katsaros, K. B., and Businger, J. A: Bulk parameterization of air-sea exchanges of heat and water vapor including the molecular constraints at the interface, *J. Atmos. Sci.*, 36, 1722–1735, 1979.
- Lyard, F., Lefevre, F., Letellier, T., and Francis, O.: Modelling the global ocean tides: modern insights from FES2004.  
930 *Ocean Dyn.*, 56 (5), 394–415. <https://doi.org/10.1007/s10236-006-0086-x>, 2006.
- Madec, G., and Imbard, M.: A global ocean mesh to overcome the north pole singularity. *Clim. Dyn.*, 12, 381–388, 1996.
- Madec, G., and the NEMO Team: NEMO ocean engine. Note du Pole de modélisation, Institut Pierre-Simon Laplace (IPSL), France, ISSN No 1288–1619. 27, 2016.
- Masson, V., Le Moigne, P., Martin, E., Faroux, S., Alias, A., Alkama, R., Belamari, S., Barbu, A., Boone, A., Bouysse, F.,  
935 Brousseau, P., Brun, E., Calvet, J.C., Carrer, D., Decharme, B., Delire, C., Donier, S., Essaouini, K., Gibelin, A.L., Giordani, H., Habets, F., Jidane, M., Kerdraon, G., Kourzeneva, E., Lafaysse, M., Lafont, S., Lebeaupin-Brossier, C., Lemosu, A., Mahfouf, J.-F., Marguinaud, P., Mokhtari, M., Morin, S., Pigeon, G., Salgado, R., Seity, Y., Taillefer, F., Tanguy, G., Tulet, P., Vincendon, B., Vionnet, V. and Voldoire, A.: The SURFEXv7.2 land and ocean surface platform for coupled or offline simulation of Earth surface variables and fluxes, *Geosci. Model Dev.*, 6, 929–960,  
940 <https://doi.org/10.5194/gmd-6-929-2013>, 2013.
- [Mazza, E., Ulbrich, U. and Klein, R.: The tropical transition of the October 1996 medicane in the western Mediterranean Sea: a warm seclusion event, \*Mon. Weather Rev.\*, 145, 2575–2595, 2017.](#)
- McTaggart-Cowan, R., Davies, E. L., Fairman Jr, J. G., Galarneau Jr, T. J., and Schultz, D. M.: Revisiting the 26.5 C sea surface temperature threshold for tropical cyclone development. *Bull. American Meteorol. Soc.*, 96(11), 1929–1943,  
945 2015.
- Mesinger, F. and Arakawa, A.: Numerical Methods Used In Atmospheric Models, Global Atmospheric Research Program Publication Series 17(1), 1976
- Miglietta, M. M., Moscatello, A., Conte, D., Mannarini, G., Lacorata, G., and Rotunno, R: Numerical analysis of a Mediterranean “hurricane” over south-eastern Italy: Sensitivity experiments to sea surface temperature, *Atmos. Res.*,  
950 101, 412–426, 2011.
- Miglietta, M.M., Laviola, S., Malvaldi, A., Conte, D., Levizzani, V. and Price, C.: Analysis of tropical-like cyclones over the Mediterranean Sea through a combined modelling and satellite approach, *Geophys. Res. Lett.*, 40, 2400–2405, 2013.
- Miglietta, M.M., Cerrai, D., Laviola, S., Cattani, E. and Levizzani, V.: Potential vorticity patterns in Mediterranean “hurricanes”. *Geophys. Res. Lett.*, 44, 2537–2545, 2017.

- 955 Miglietta, M.M., and Rotunno, R.: Development mechanisms for Mediterranean tropical-like cyclones (medicanes), Q. J. Roy. Meteorol. Soc., 1–17. <https://doi.org/10.1002/qj.3503>, 2019.
- Morcrette, J.-J.: Radiation and cloud radiative properties in the ECMWF operational weather forecast model. J. Geophys. Res., 96D, 9121–9132, 1991.
- Moscattello, A., Miglietta, M.M. and Rotunno, R.: Numerical analysis of a Mediterranean “hurricane” over southeastern  
960 Italy, Mon. Weather Rev., 136, 4373–4397, 2008.
- Myers, J. L., Well, A. D., and Lorch, R.F. Jr: Research Design and Statistical Analysis (3rd ed.), Taylor and Francis Eds., New York, 2010.
- Noyelle, R., Ulbrich, U., Becker, N., and Meredith, E. P.: Assessing the impact of sea surface temperatures on a simulated medicane using ensemble simulations, Nat. Hazards Earth Syst. Sci., 19, 941–955, [https://doi.org/10.5194/nhess-19-941-](https://doi.org/10.5194/nhess-19-941-2019)  
965 2019, 2019.
- Pergaud, J., Masson, V., Malardel, S. and Couvreux, F.: A parameterization of dry thermals and shallow cumuli for mesoscale numerical weather prediction, Bound.-Layer. Meteor., 132, 83–106, doi: 10.1007/s10546-009-9388-0, 2009.
- Picornell, M. A., Campins, J., and Jansà, A.: Detection and thermal description of medicanes from numerical simulation, Nat. Hazards Earth Syst. Sci, 14, 1059–1070, 2014.
- 970 Pytharoulis, I.: Analysis of a Mediterranean tropical-like cyclone and its sensitivity to the sea surface temperatures. Atmospheric Research, 208, 167–179, 2018.
- Rainaud, R., Lebeaupin Brossier, C., Ducrocq, V., and Giordani, H.: High-resolution air-sea coupling impact on two heavy precipitation events in the Western Mediterranean. Quart. J. Roy. Meteor. Soc., 143, 2448–2462, <https://doi.org/10.1002/qj.3098>, 2017.
- 975 Reale, O. and Atlas, R.: Tropical cyclone-like vortices in the extratropics: observational evidence and synoptic analysis. Weather and Forecasting, 16, 7–34, 2001.
- Redelsperger, J.L. and Sommeria, G.: Three-dimensional simulation of a convective storm: Sensitivity studies on subgrid parameterization and spatial resolution, J. Atmos. Sci., 43, 2619–2635, [https://doi.org/10.1175/1520-0469\(1986\)043,](https://doi.org/10.1175/1520-0469(1986)043,2619:TDSOAC.2.0.CO;2)  
2619:TDSOAC.2.0.CO;2, 1986.
- 980 Redelsperger, J.-L., Mahé, F. and Carlotti, P.: A simple and general subgrid model suitable both for surface layer and free-stream turbulence. Bound.-Layer. Meteor., 101, 375–408. <https://doi.org/10.1023/A:1019206001292>, 2001.
- Reed, R.J., Kuo, Y.-H., Albright, M.D., Gao, K., Guo, Y.-R. and Huang, W.: Analysis and modeling of a tropical-like cyclone in the Mediterranean Sea, Meteorol. Atmos. Phys., 76, 183–202, 2001.
- Renault, L., Chiggiato, J., Warner, J.C., Gomez, M., Vizoso, G. and Tintoré, J.: Coupled atmosphere-ocean-wave  
985 simulations of a storm event over the Gulf of Lion and Balearic Sea, J. Geophys. Res., 117, C09019, doi:10.1029/2012JC007924, 2012.
- Ricchi, A., Miglietta, M.M., Barbariol, F., Benetazzo, A., Bergamasco, A., Bonaldo, D., Cassardo, C., Falcieri, F.M., Modugno, G., Russo, A., Sclavo, M. and Carniel, S.: Sensitivity of a Mediterranean tropical-like cyclone to different model configurations and coupling strategies, Atmosphere, 8(5), 92, 1–32, <https://doi.org/10.3390/atmos8050092>, 2017.
- 990 Rotunno, R. and Emanuel, K.: An air–sea interaction theory for tropical cyclones. Part II: Evolutionary study using a nonhydrostatic axisymmetric numerical model. J. Atmos. Sci., 44, 542–561, 1987.
- Roulet, G., and Madec, G.: Salt conservation, free surface and varying levels: a new formulation for ocean general circulation models. J. Geophys. Res. 105 (C10), 23927–23942. <https://doi.org/10.1029/2000JC900089>, 2000.

- Schade, L. R., and Emanuel, K. A.: The ocean's effect on the intensity of tropical cyclones: Results from a simple coupled  
 995 atmosphere–ocean model. *J. Atmos. Sci.*, 56, 642–651, 1999.
- Schär, C., and Wernli, H.: Structure and evolution of an isolated semi-geostrophic cyclone. *Q. J. R. Meteorol. Soc.*,  
 119(509), 57-90, 1993.
- Seity, Y., Brousseau, P., Malardel, S., Hello, G., Bénard, P., Bouttier, F., Lac, D. and Masson, V.: The AROME-France  
 convective-scale operational model. *Mon. Weather Rev.*, 139, 976–991. <https://doi.org/10.1175/2010MWR3425.1>, 2011.
- 1000 Tibaldi, S., Buzzi, A. and Speranza, A.: Orographic cyclogenesis, in *Extratropical cyclones, The Palmen Memorial volume*,  
 edited by: Newton, C., and Holopainen, E. O. American Meteorological Society, Boston, 107-127, 1990.
- Tous, M. and Romero, R.: Meteorological environments associated with medicane development, *Int. J. Climatol.*, 33, 1–14,  
 2013.
- Trenberth, K.: Uncertainty in hurricanes and global warming, *Science*, 308 (5729), 1753-1754,  
 1005 [doi:10.1126/science.1112551](https://doi.org/10.1126/science.1112551), 2005.
- Voldoire, A., Decharme, B., Pianezze, J., Lebeaupin Brossier, C., Sevault, F., Seyfried, L., Garnier, V., Bielli, S., Valcke, S.,  
 Alias, A., Accensi, M., Arduin, F., Bouin, M.-N., Ducrocq, V., Faroux, S., Giordani, H., Léger, F., Marsaleix, P.,  
 Rainaud, R., Redelsperger, J.-L., Richard, E., and Riette, S.: SURFEX v8.0 interface with OASIS3-MCT to couple  
 1010 atmosphere with hydrology, ocean, waves and sea-ice models, from coastal to global scales, *Geosci. Model Dev.*, 10,  
 4207–4227, <https://doi.org/10.5194/gmd-10-4207-2017>, 2017.

Tables

	$U_{10}$	$\theta$	SST	$q$
$H+LE$	0.66	-0.20	0.35	0.48
$LE$	0.65	0.10	0.36	0.33
$H$	0.38	-0.70	0.21	
$U_{10}$		-0.10	-0.25	0.84
$\theta$			-0.04	-0.03
SST				-0.18

1015 **Table 1:** Spearman's rank correlations between the enthalpy flux, latent and sensible heat flux and related parameters (10 m wind speed  $U_{10}$ , potential temperature at 10 m  $\theta$ , SST and humidity at 10 m  $q$ ) at 09:00 UTC on 7 November, from the CPL simulation, on the EF600 area.

	$U_{10}$	$\theta$	SST	$q$
$H+LE$	0.62	-0.14	0.28	0.49
$LE$	0.49	0.22	0.42	0.23
$H$	0.55	-0.72	-0.10	
$U_{10}$		-0.19	-0.38	0.87
$\theta$			0.41	-0.32
SST				-0.34

1020 | **Table 2:** Same as Table 1 at 13:00 UTC on 7 November.

1025

	$U_{10}$	$\theta$	SST	$q$
$H+LE$	0.31	-0.09	0.32	0.17
$LE$	0.16	0.26	0.46	-0.03
$H$	0.37	-0.75	-0.20	
$U_{10}$		-0.02	-0.52	0.93
$\theta$			0.40	-0.04
SST				-0.49

1030 | **Table 3:** Same as ~~st~~ Table 1 at 18:00 UTC on 7 November.

Figures

1035

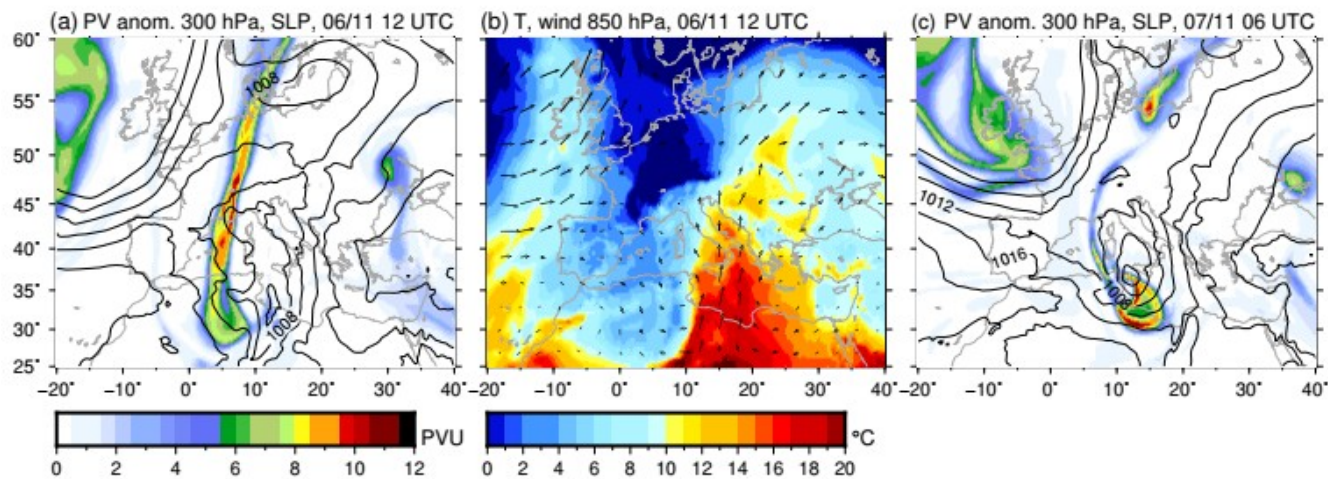
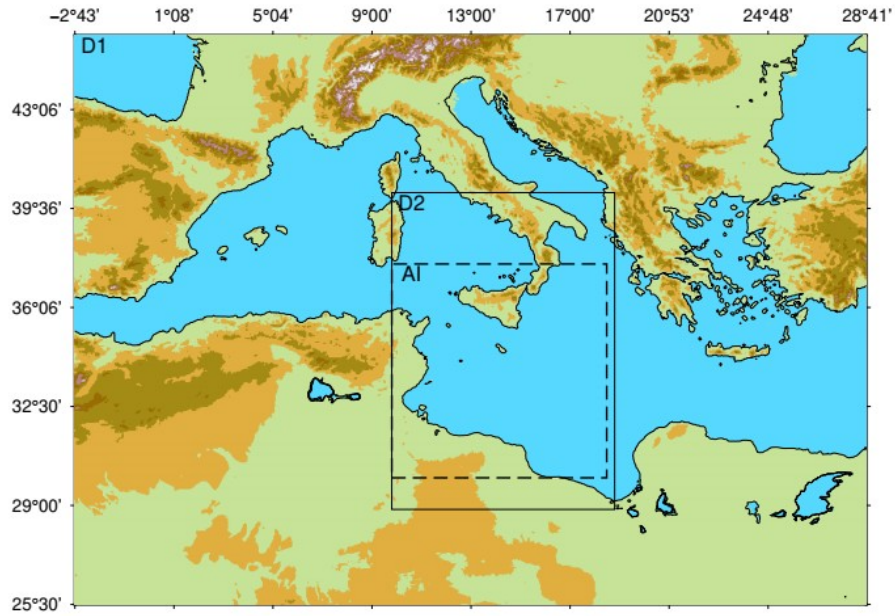


**Figure 1:** Potential vorticity (PV) anomaly at 300 hPa (colour scale) and SLP (isocontours every 4 hPa) at 12:00 UTC on 6 November (a) and 06:00 UTC on 7 November (c), temperature (colour scale, °C) and wind at 850 hPa at 06:00 UTC on 6 November (b) from the ERA5 reanalysis.

1040

1045

1050



1055 **Figure 2:** Map of the large-scale domain D1, with the domain D2 indicated by the solid-line frame and the area of interest (AI) indicated  
1060 by the dashed-line frame.

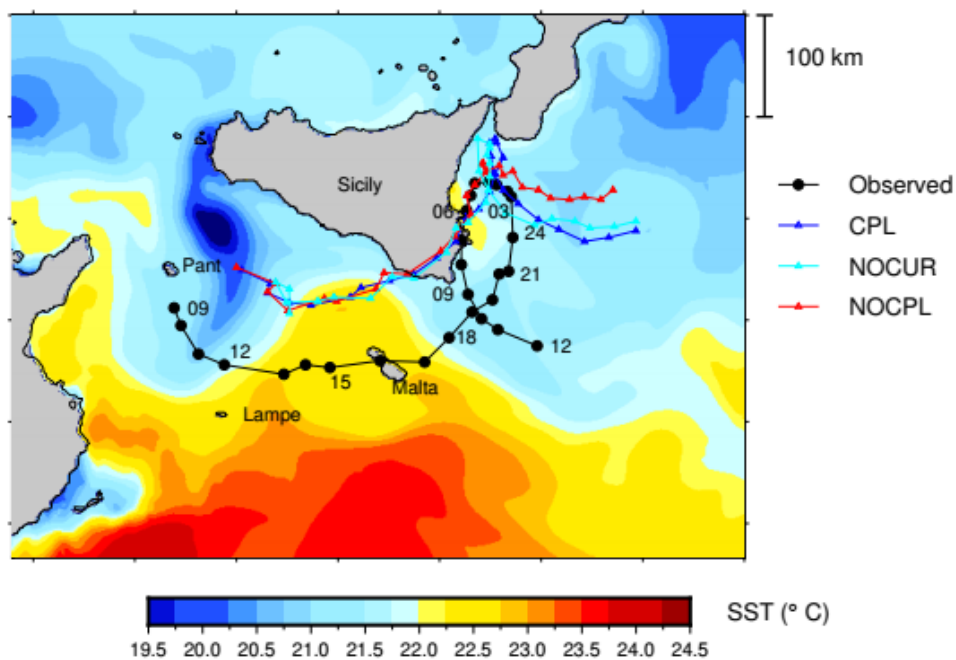
1060



1065

1070

1075



1080

**Figure 3:** Comparison of the simulated tracks (triangles) of the non-coupled run (NOCPL, red), coupled run with SST only (NOCUR, cyan) and fully coupled run (CPL, blue) with the best track (black closed circles) based on observations as in Cioni et al., (2018). The position is shown every hour with time labels every 3 h, starting at 09:00 UTC on 7 November until 12:00 UTC on 8 November. In colours, initial Sea Surface Temperature (SST, °C) at 01:00 UTC on 7 November.

1085

1090

1095

1100

1105

1115

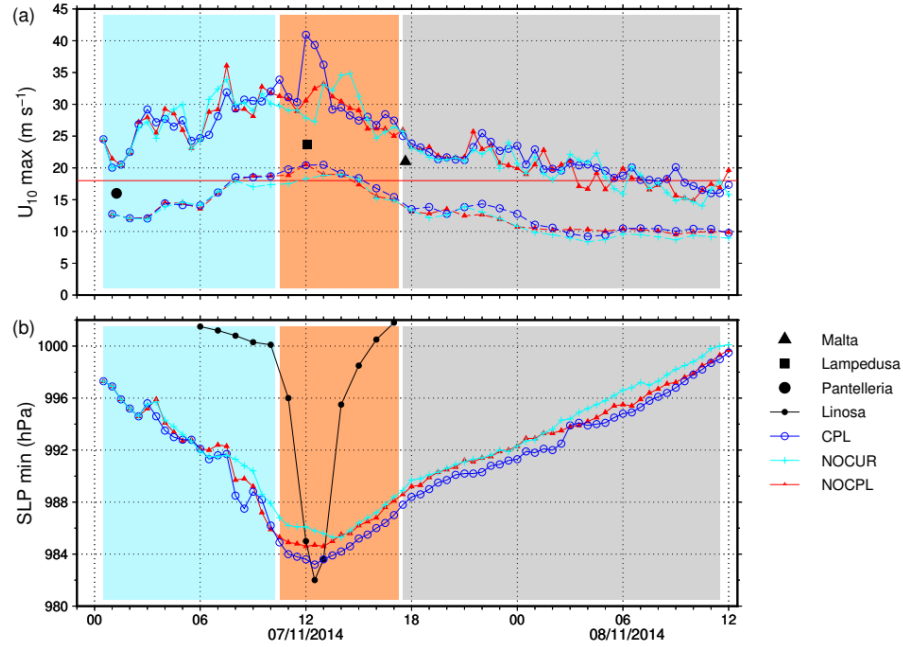
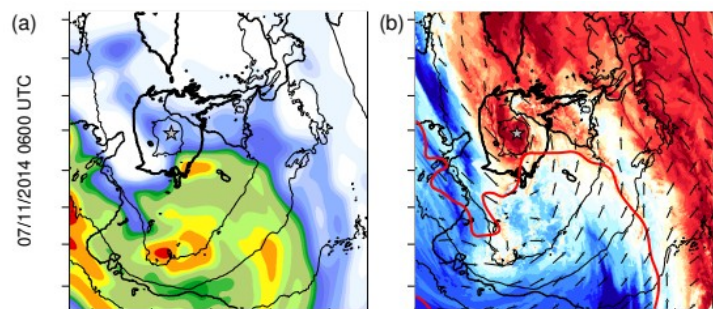
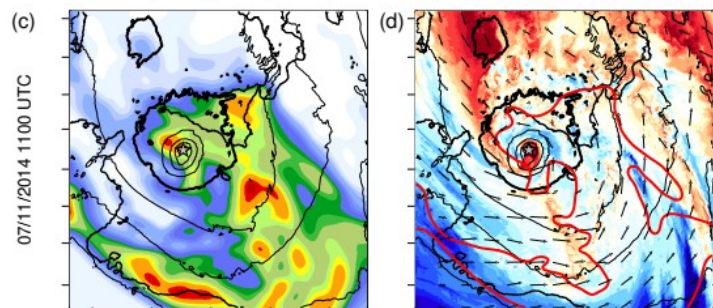


**Figure 4:** Time series of the maximum of the 10 m wind speed, and of the 10 m wind averaged over a 100 km radius around the cyclone centre (a) and minimum sea-level pressure (b) as obtained in the different simulations on the 7 November and 8 November until 12:00 UTC. The thin red line in (a) indicates the  $18 \text{ m s}^{-1}$  wind speed threshold. The background shading (here and in the following time-series plots) indicates the development (light blue), mature (orange) and decay (grey) phases. The observations of SLP in Linosa (black plain circles) are shown for comparison in (b), the observations of wind speed from Malta, Lampedusa and Pantelleria are shown in (a) – see text.

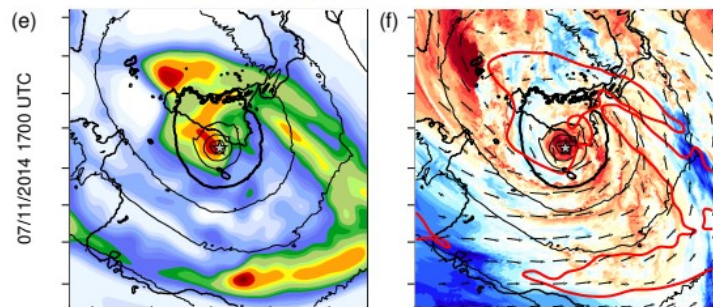
1120



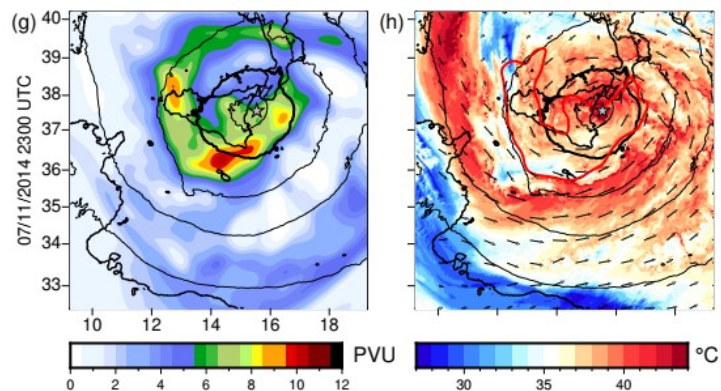
1125



1130



1135



1140

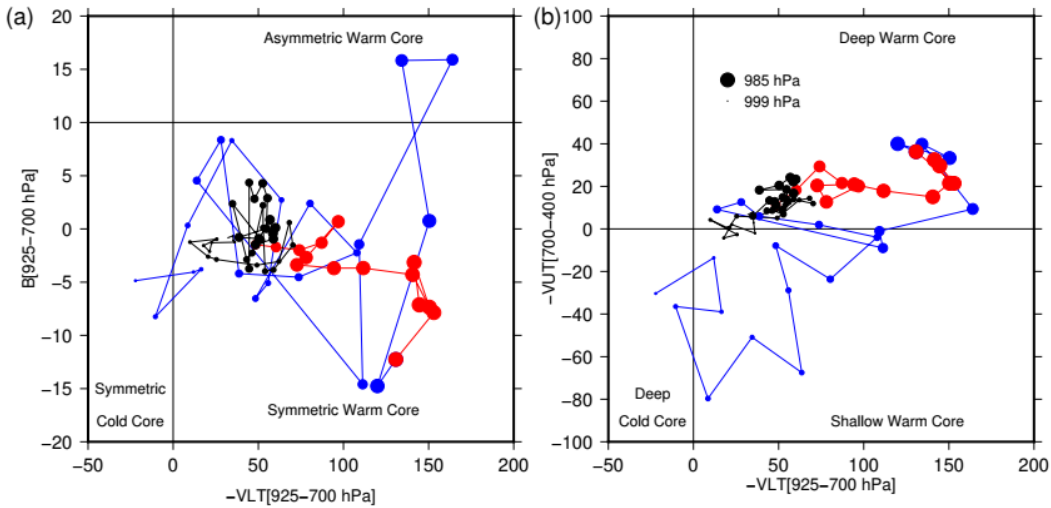
1145

**Figure 5:** Potential vorticity at 300 hPa (colour scale) and SLP (isocontours every 4 hPa, the 1000 hPa isobar is in bold), (a, c, e, g) and equivalent potential temperature (°C, colour scale) and wind at 850 hPa, SLP, and 6 PVU at 300 hPa isocontours (red), (b, d, f, h) from the NOCPL simulation.

1150

1155

1160



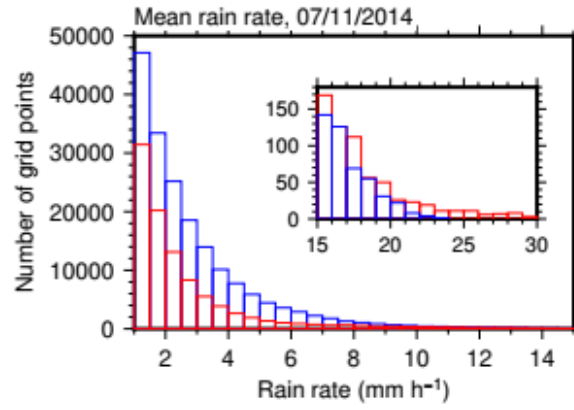
1165

**Figure 6:** Phase diagram of the NOCPL simulated cyclone from 01:00 UTC on 7 November till 12:00 UTC on 8 November, with low-tropospheric thickness asymmetry inside the cyclone ( $B$ ) with respect to low-tropospheric thermal wind ( $-V_{LT}$ ) (a), and upper-tropospheric thermal wind ( $-V_{UT}$ ) with respect to low-tropospheric thermal wind (b). The development phase is in blue, the mature phase in red, and the decay phase in black.

1170

1175

1180



1185

**Figure 7:** Histogram of the mean rain rate distribution (in number of grid points) for the development (blue) and mature (red) phases in the NOCPL simulation. The enclosed figure shows a zoom on the highest rates.

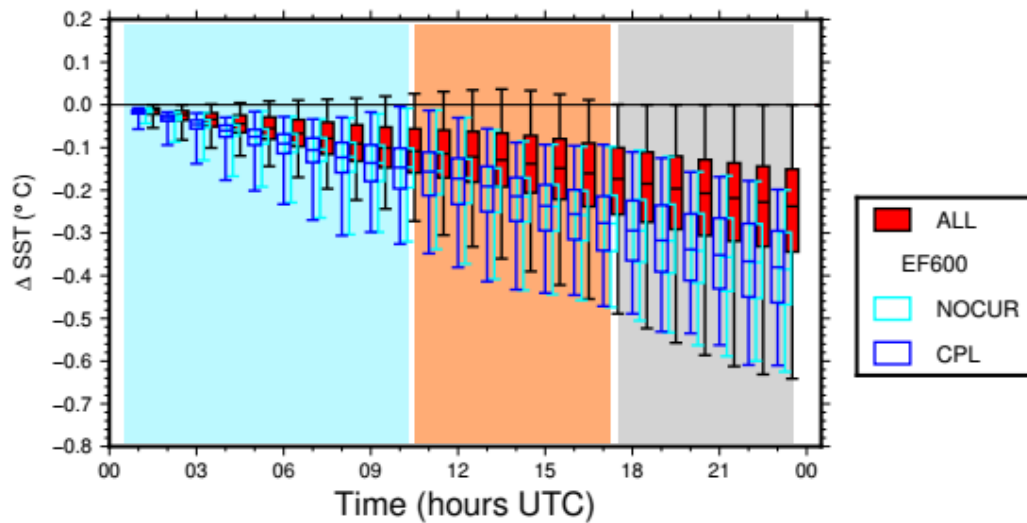


**Figure 8:** Time series of the median differences between the SST in the CPL and NOCPL simulations, on the whole domain (red) and on the EF600 area (blue, see text for definition), on the 7 November. The boxes indicates the 25 and 75% quantiles and the whiskers the 5 and 95% quantiles. ~~T~~Are also shown the SST differences on EF600 between the NOCUR and NOCPL simulations are also shown (cyan). Some ~~of the~~ boxes have been slightly shifted horizontally for clarity.

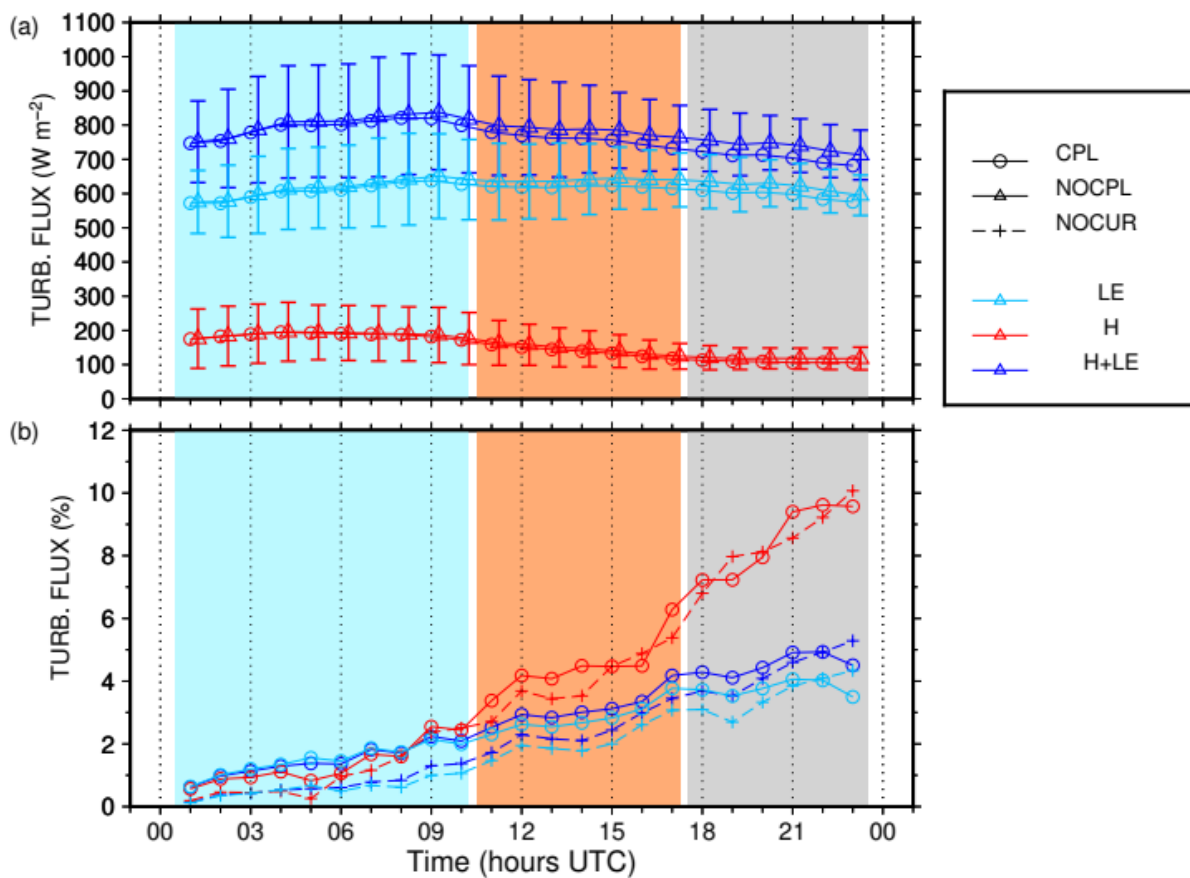
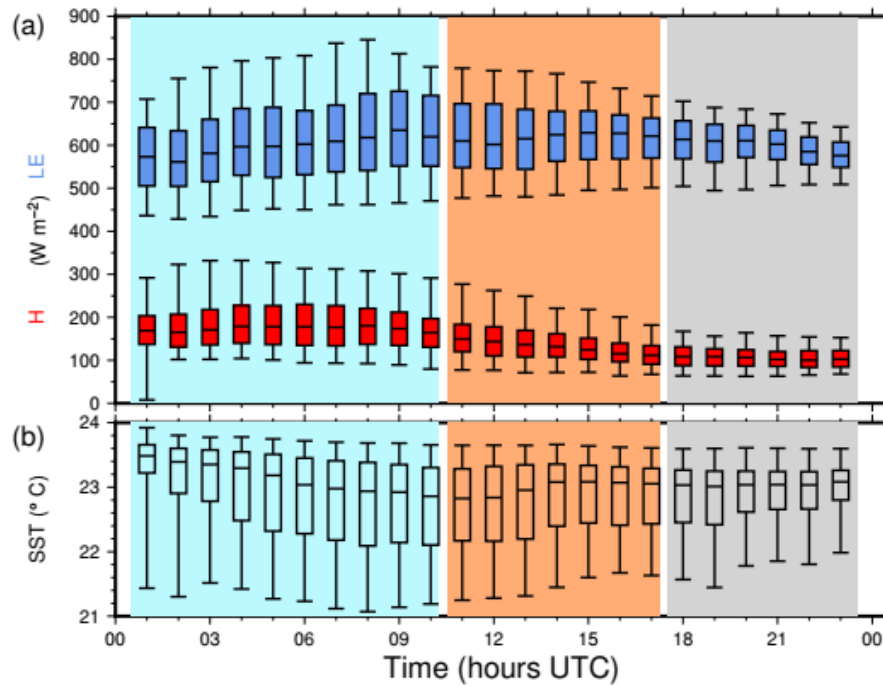


**Figure 9:** Time series of the mean values and standard deviation (error bars) of the total turbulent heat flux (blue), latent (cyan) and sensible heat flux (red) in the CPL (open circles) and NOCPL (triangles) simulations (a) and of the mean difference between CPL and NOCPL turbulent fluxes (open circles, same colour code) and between NOCUR and NOCPL turbulent fluxes, in percent relative to the NOCPL values (b) on the EF600 area.

1215

1220

1225



1230 | **Figure 10:** Time series of the median values of latent (blue) and sensible heat fluxes (red, a) and of SST (b) on the EF600 area (see text) [in the NOCPL run](#) on the 7 November. The boxes corresponds to the 25 and 75% quantiles, the whiskers to the 5 and 95% quantiles.



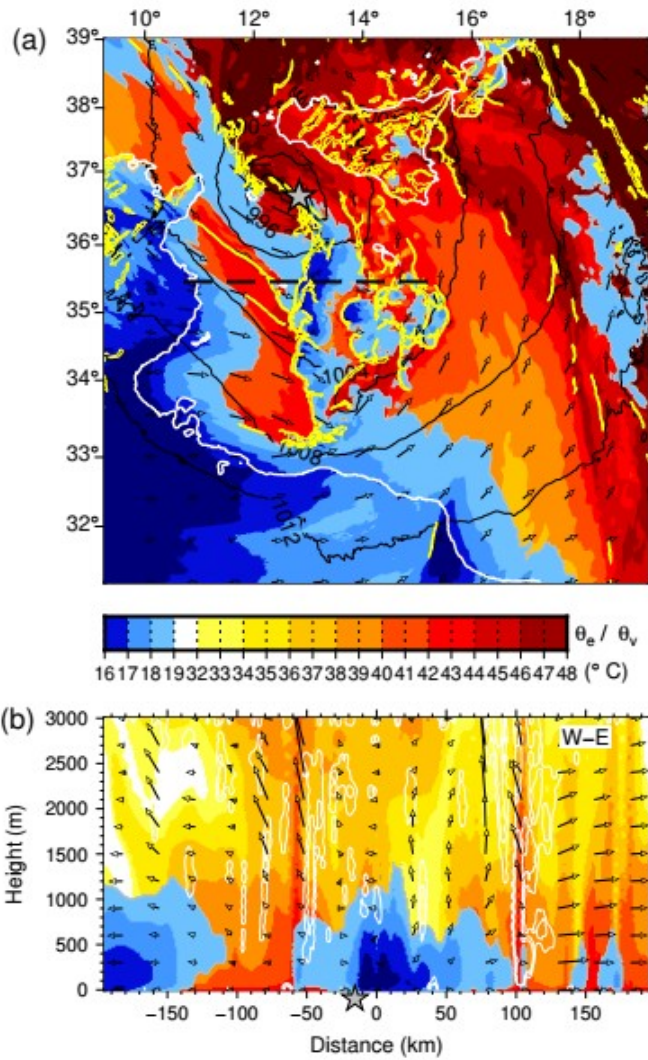


**Figure 11:** Map of equivalent potential temperature (warm colors) and virtual potential temperature below 19 °C (blue shades) at first level, horizontal convergence rate above  $1 \times 10^{-3} \text{ m s}^{-2}$  at 100 m (yellow contours), 10 m wind (arrows) and SLP (black contours) at 08:30 UTC on 7 November (a), and vertical cross-section of equivalent potential temperature and virtual potential temperature (colour scale), tangential wind (black vectors, the vertical component is amplified by a factor 20), potential vorticity anomaly (white contour at 5 PVU) along a west-east transect (b) (dashed line in (a)). The grey stars indicate the position of the SLP minimum.

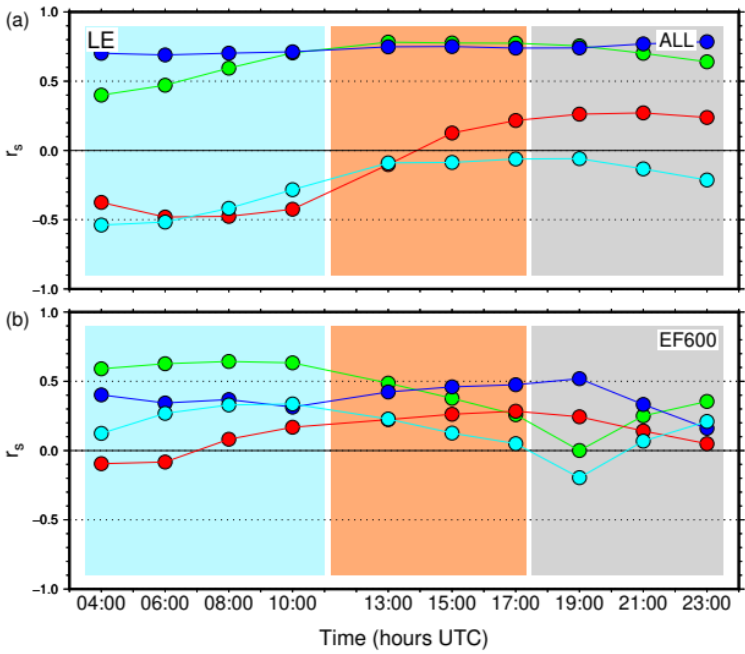


**Figure 12:** Time series of Spearman's rank-order correlation  $r_s$  between the latent heat flux  $LE$  and 10 m wind speed (green), potential temperature at 10 m (red), SST (blue) and specific humidity at 2 m (cyan) on the whole domain (a) and for the EF600 area (b), in the CPL simulation.

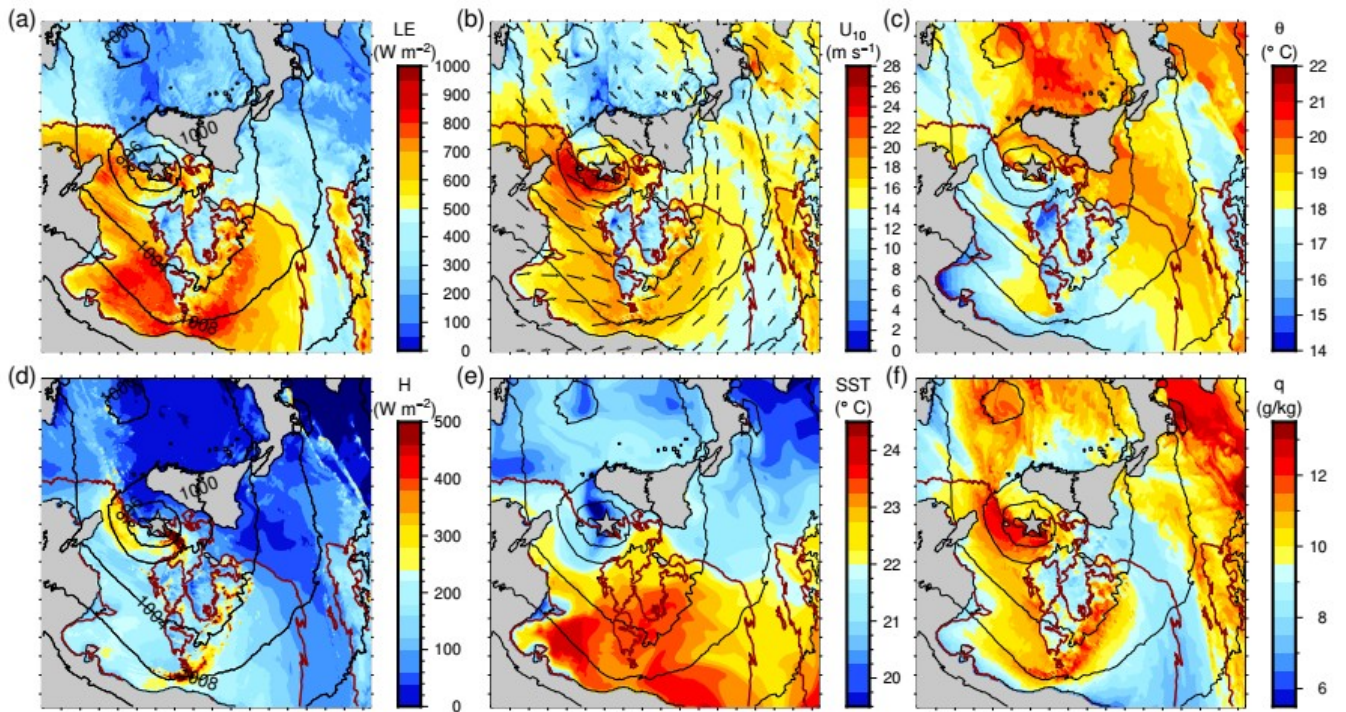


**Figure 13:** Maps of the total turbulent heat fluxes  $LE$  (a),  $H$  (d), the 10 m wind  $U_{10}$  (b), the 10 m potential temperature (c), the SST (e) and the specific humidity at 2 m (f) at 09:00 UTC on 7 November, in the CPL simulation.

1290

1295

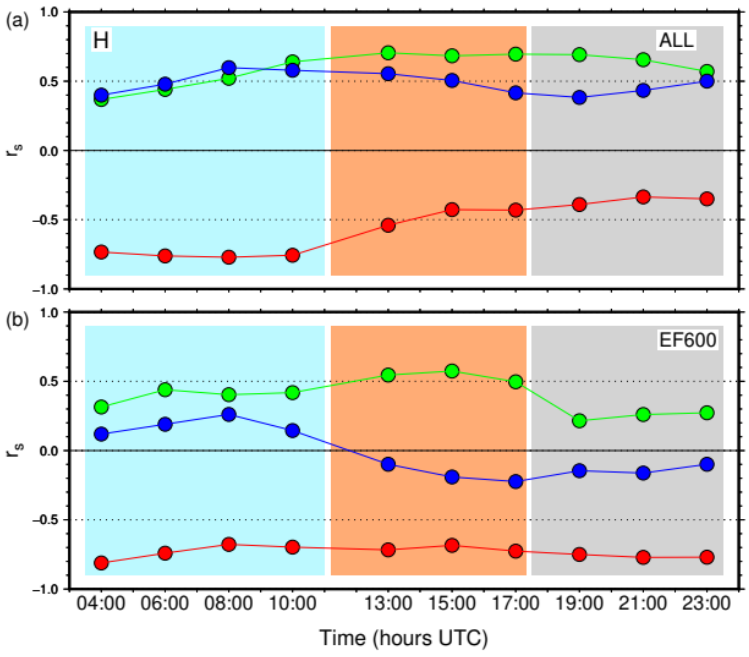


**Figure 14:** Same as Figure 12 but between the sensible heat flux  $H$  and 10 m wind speed (green), potential temperature at 10 m (red), and SST (blue) on the whole domain (a) and EF600 area (b), in the CPL simulation.

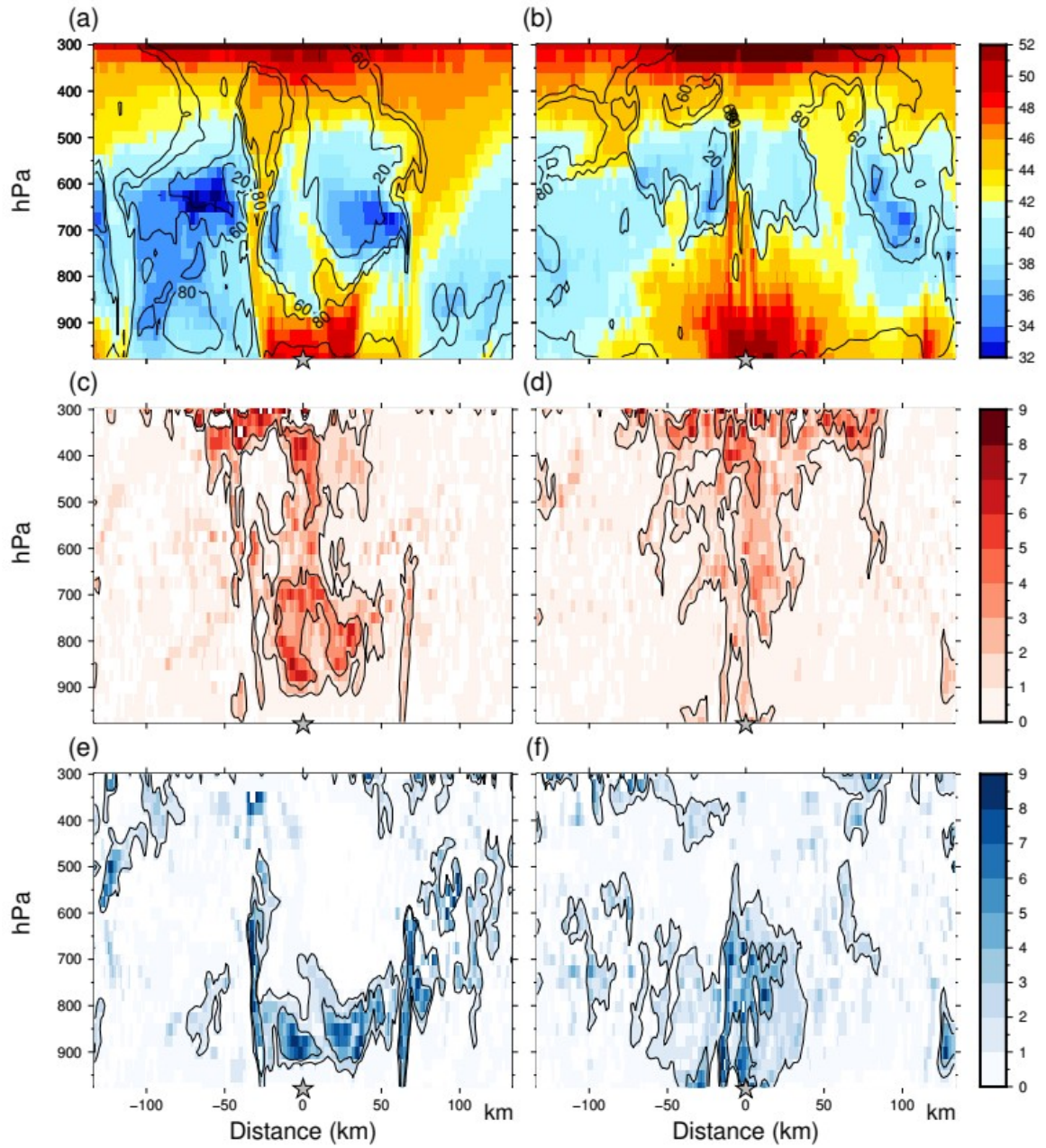


1315

1320

1325

1330



1335 **Figure 15:** Vertical cross-sections of equivalent potential temperature  $\theta_e$  (°C, colour scale) and relative humidity (%), (a,b), DPV (intensity), (c,d) and WPV (intensity), (e,f) on a west-east transect across the cyclone centre, at 13:00 (a,c,e) and 18:00 UTC (b,d,f) on 7 November, in the CPL simulation. The black contours in (c) to (f) correspond to intensities 1 and 3 (as defined in Miglietta et al., 2017).

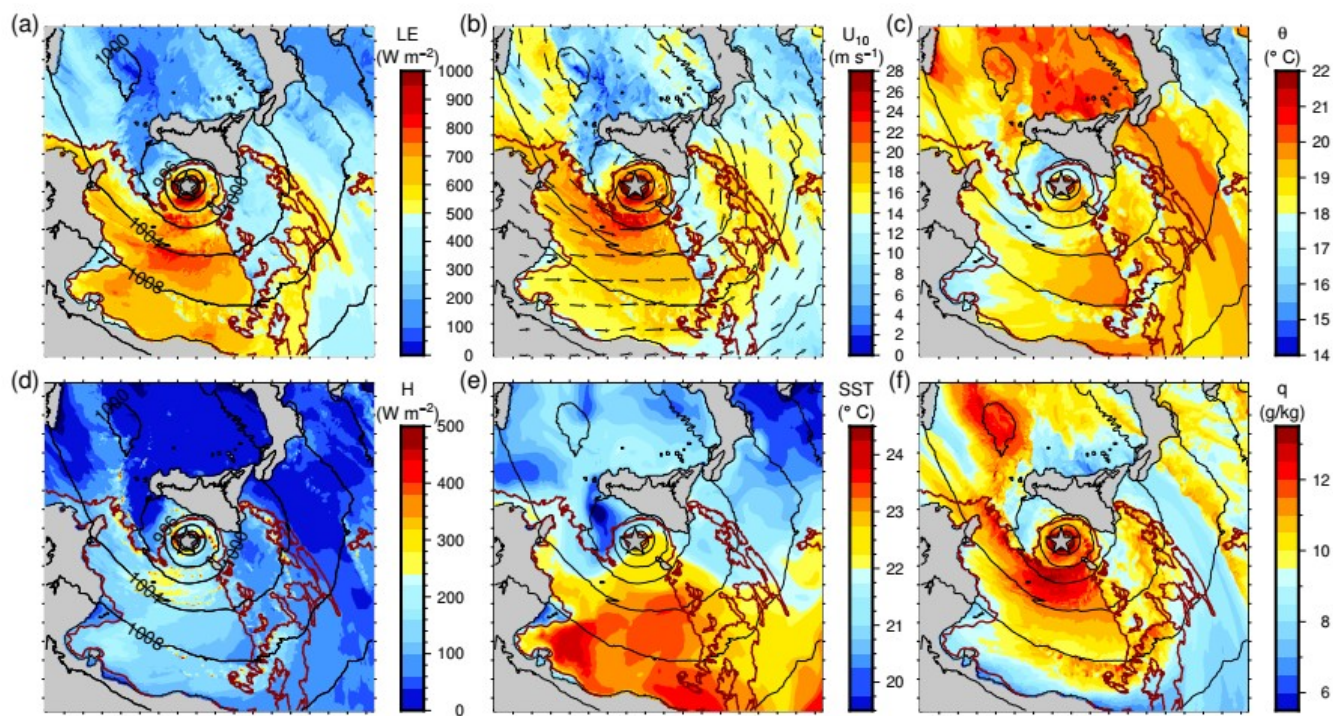


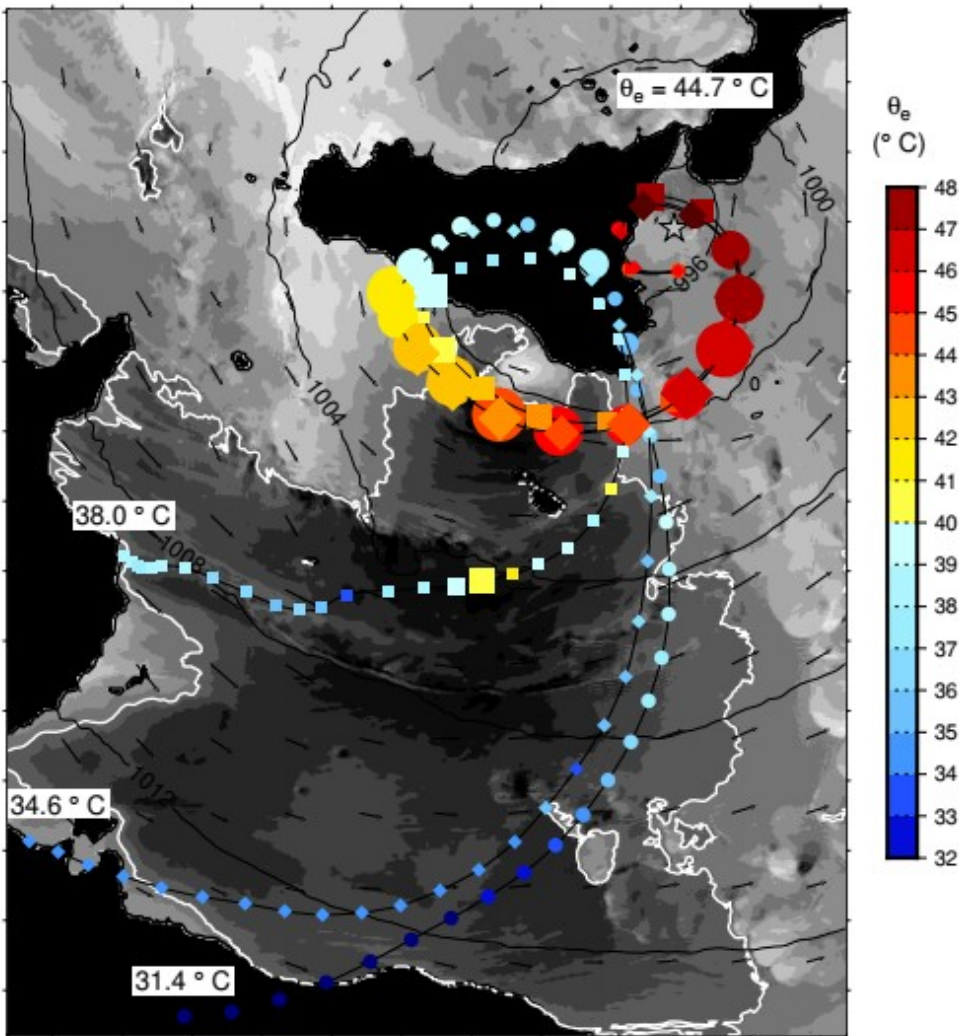
**Figure 16:** Same as Figure 13 but at 13:00 UTC on 7 November.

1345

1350

1355

1360

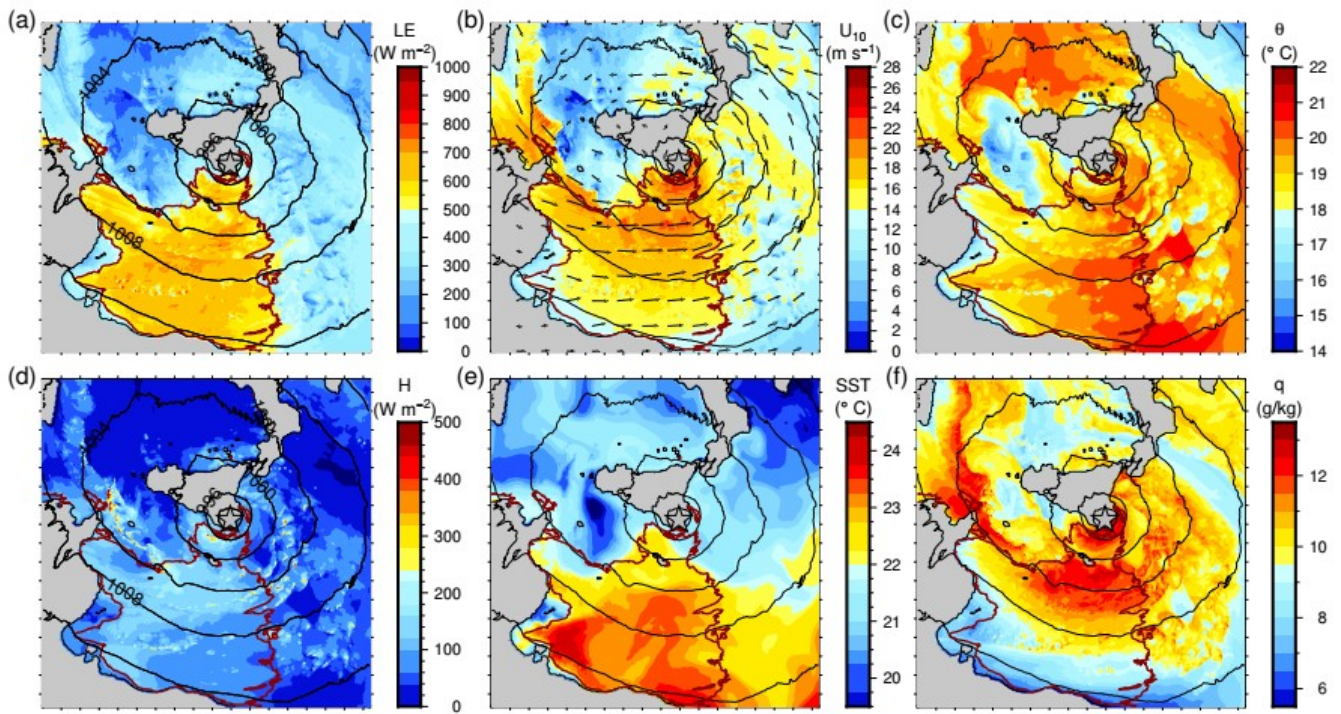


1365

**Figure 17:** Map of the backtrajectories of air parcels arriving south of the cyclone centre at 23:00 UTC on 7 November, 1500 m above sea level, at 3 different levels (circles, squares and diamonds). The first point of the trajectories correspond to the start of the D2 domain simulation (00 UTC the 07 November). The colour scale indicates the equivalent potential temperature ( $^{\circ}\text{C}$ ) and the size of the symbol is inversely proportional to altitude between 0 and 1000 m, and constant above 1000 m. Are also shown the values of the final equivalent potential temperature, of the initial equivalent potential temperatures, the wind field at 900 hPa (black vectors), and the surface enthalpy flux (grey shades) with a threshold at  $600\text{ W m}^{-2}$  (white contour) at 15:30 UTC when the particles arrive at sea south of Sicily.

1370



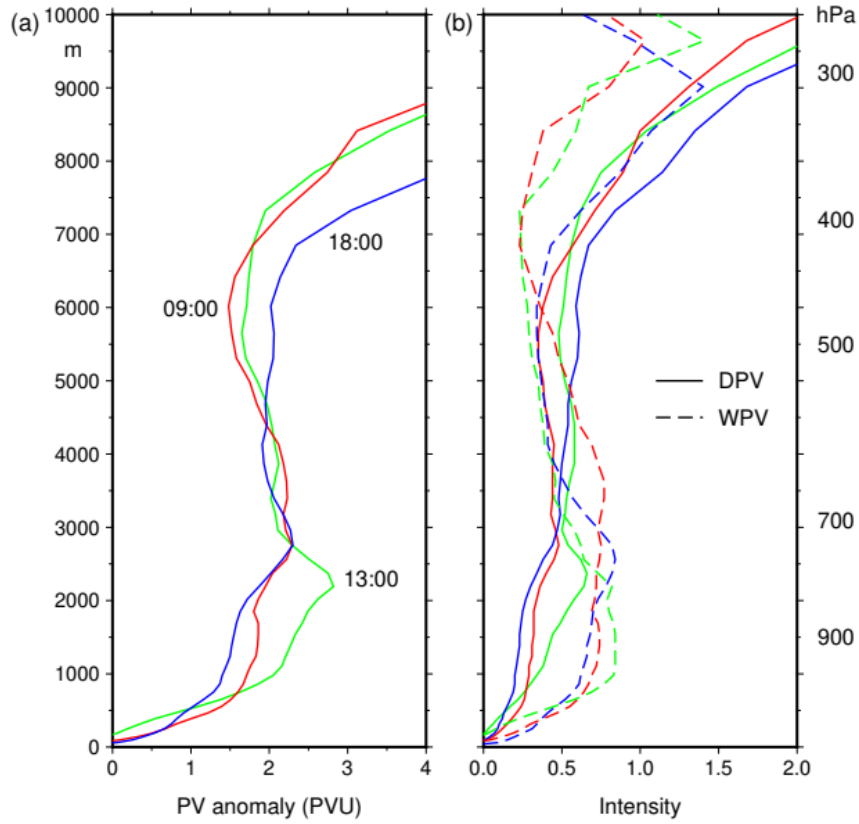


1375 **Figure 18:** Same as Figure 13 but at 18:00 UTC on 7 November.

1380

1385

1390



1395 **Figure 19:** Vertical profiles of PV (a), and DPV and WPV (b) averaged within a 100-km radius circle around the cyclone centre at 09:00 (red), 13:00 (green) and 18:00 UTC (blue) on 7 November, in the CPL simulation.